Article

Immunity

Adventitial Stromal Cells Define Group 2 Innate Lymphoid Cell Tissue Niches

Graphical Abstract

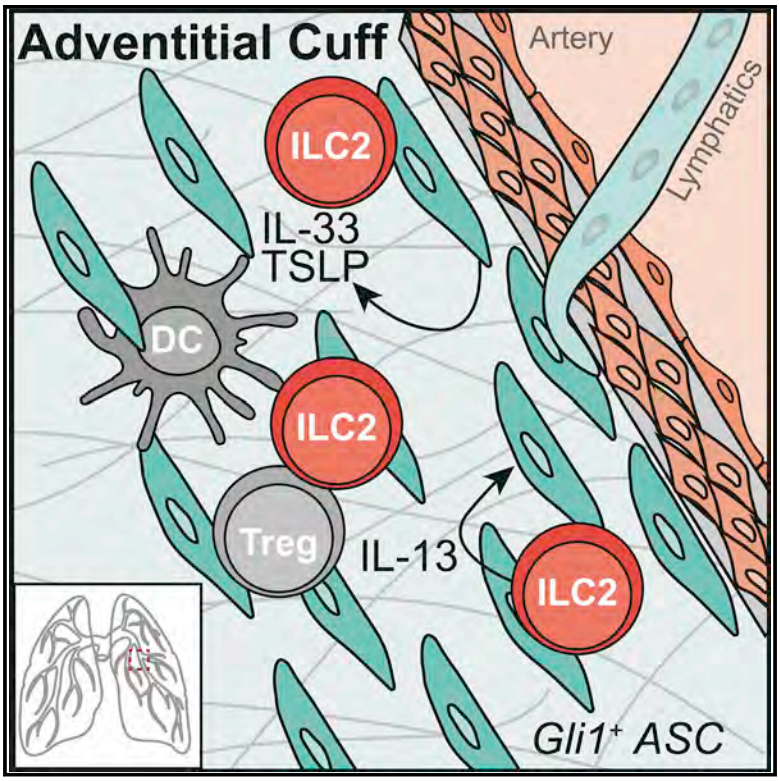

Authors

Madelene W. Dahlgren, Stephen W. Jones, Kelly M. Cautivo, ..., Matthew F. Krummel, Tien Peng, Ari B. Molofsky

Correspondence

ari.molofsky@ucsf.edu

In Brief

Tissue-resident type 2 lymphocytes are involved in both physiologic and pathologic responses, yet their physical tissue niches are poorly described. Here, Dahlgren et al. identify a population of perivascular fibroblast-like stromal cells that express IL-33 and TSLP as local regulators of ILC2s and type 2 immunity.

Highlights

- 3D imaging defines ILC2 niches in perivascular regions of multiple tissues
- ILC2s localize with fibroblast-like adventitial stromal cells (ASCs)
- Lung ASCs produce IL-33 and TSLP to support ILC2 and Th2s
- ILC2s promote ASC expansion and IL-33 production after helminth infection

Dahlgren et al., 2019, Immunity *50*, 707–722
March 19, 2019
https://doi.org/10.1016/j.immuni.2019.02.002

CellPress

Immunity
Article

Adventitial Stromal Cells Define Group 2 Innate Lymphoid Cell Tissue Niches

Madelene W. Dahlgren,[1,7] Stephen W. Jones,[1,7] Kelly M. Cautivo,[1] Alexandra Dubinin,[1] Jorge F. Ortiz-Carpena,[1] Sepideh Farhat,[1] Kevin S. Yu,[4] Katharine Lee,[4] Chaoqun Wang,[2] Anna V. Molofsky,[5] Aaron D. Tward,[4] Matthew F. Krummel,[3] Tien Peng,[2] and Ari B. Molofsky[1,6,8,*]

[1]Department of Laboratory Medicine, University of California, San Francisco, San Francisco, CA 94143, USA
[2]Department of Medicine, University of California, San Francisco, San Francisco, CA 94143, USA
[3]Department of Pathology, University of California, San Francisco, San Francisco, CA 94143, USA
[4]Department of Otolaryngology–Head and Neck Surgery, University of California, San Francisco, San Francisco, CA 94143, USA
[5]Department of Psychiatry, University of California, San Francisco, San Francisco, CA 94143, USA
[6]Diabetes Center, University of California, San Francisco, San Francisco, CA 94143, USA
[7]These authors contributed equally
[8]Lead Contact
*Correspondence: ari.molofsky@ucsf.edu
https://doi.org/10.1016/j.immuni.2019.02.002

SUMMARY

Type 2 lymphocytes promote both physiologic tissue remodeling and allergic pathology, yet their physical tissue niches are poorly described. Here, we used quantitative imaging to define the tissue niches of group 2 innate lymphoid cells (ILC2s), which are critical instigators of type 2 immunity. We identified a dominant adventitial niche around lung bronchi and larger vessels in multiple tissues, where ILC2s localized with subsets of dendritic and regulatory T cells. However, ILC2s were most intimately associated with adventitial stromal cells (ASCs), a mesenchymal fibroblast-like subset that expresses interleukin-33 (IL-33) and thymic stromal lymphopoietin (TSLP). *In vitro*, ASCs produced TSLP that supported ILC2 accumulation and activation. ILC2s and IL-13 drove reciprocal ASC expansion and IL-33 expression. During helminth infection, ASC depletion impaired lung ILC2 and Th2 cell accumulation and function, which are in part dependent on ASC-derived IL-33. These data indicate that adventitial niches are conserved sites where ASCs regulate type 2 lymphocyte expansion and function.

INTRODUCTION

Type 2 immunity drives both beneficial responses that restrict helminth infections and pathologic responses that promote asthma, atopic dermatitis, and allergy. Group 2 innate lymphoid cells (ILC2s) are critical initiators of type 2 allergic immunity, defined by elevated systemic immunoglobulin E (IgE), tissue eosinophils, M2 alternatively activated macrophages, and epithelial cell subsets (e.g., goblet cells and tuft cells) that ultimately mediate tissue remodeling (Klose and Artis, 2016; Schuijs and Halim, 2018). Recent work supports a broadening of the physiologic roles for ILC2s and type 2 immunity, including promoting tissue development, metabolic homeostasis, physiologic remodeling, and wound healing (Vivier et al., 2018).

Similar to many innate lymphoid cells and innate-like T cells, ILC2s are predominantly developmentally allocated, tissue-resident lymphocytes that are long lived and integrate multiple signals to rapidly initiate local immune responses (Klose and Artis, 2016; Schuijs and Halim, 2018; Vivier et al., 2018). ILC2s are present at epithelial barriers, including the skin and gastrointestinal (GI) and respiratory tracts; however, ILC2s also reside in deep "non-barrier" tissues such as adipose, liver, central nervous system meninges, pancreas, uterus, and kidney (Nussbaum et al., 2013). After allergic challenge or helminth infection, subsets of adaptive $CD4^+$ T helper type 2 cells become tissue-resident memory (Th2 TRM) cells, can respond to tissue signals independent of antigen, and are amplifiers of allergic immunity (Endo et al., 2015; Guo et al., 2015; Van Dyken et al., 2016). Many of the upstream signals controlling ILC2s and Th2 TRM cells, including the cytokines IL-33 and thymic stromal lymphopoietin (TSLP), are locally released by tissue-resident cells and are critical regulators of allergic physiology and pathology (Cayrol and Girard, 2018; Molofsky et al., 2015a; Ziegler, 2012). This raises the question of which cells produce these and other signals that locally regulate ILC2 and Th2 TRM cell positioning and function.

Most adaptive lymphocytes interact in secondary lymphoid organs (SLOs) such as lymph nodes and spleen, where microanatomic niches regulate specialized immune functions (Chang and Turley, 2015; Rodda et al., 2018). However, the stromal niches of tissue-resident lymphocytes in non-SLO tissues have been difficult to define because of limited cell numbers and suboptimal reagents for tracking lymphocyte subsets. Stromal cells are diverse, and include pericytes that support capillaries, epithelial-like mesothelial cells that form body-cavity serosal surfaces, and heterogenous fibroblast-like mesenchymal cells (Han et al., 2018). Adventitial stromal cells (ASCs) are the major constituents of perivascular adventitial "cuffs," comprising the outermost layer of intermediate-to-large blood vessels and other tubular structures, such as lung airways (Benias et al., 2018;

Schraufnagel et al., 2003; Stenmark et al., 2013). Adventitial cuffs are diverse interstitial spaces rich in collagens, extracellular matrix components, small blood vessels, neurons, progenitor cells, and immune cells, providing both vascular support and conduits for interstitial fluid to accumulate and drain into lymphatics. In addition to playing roles in vascular remodeling, ASCs also participate in both vascular and tissue immune responses, engaging in bi-directional conversations with macrophages and dendritic cells (DCs) in settings of inflammation and ultimately contributing to the expansion of tertiary lymphoid organs (TLOs) (Stenmark et al., 2013).

Here, we used tissue clearing with 3D imaging (Oldham et al., 2008), image quantitation (i.e., histo-cytometry) (Gerner et al., 2012), transcriptomics, and functional assays to define ILC2 niches in the lung and multiple ''non-barrier'' tissues. We describe a dominant ILC2 niche in adventitial cuffs, where ILC2s reside in proximity to subset(s) of regulatory T (Treg) cells, DCs, and lymphatics. We identified IL-33- and TSLP-producing ASCs that are intimately associated with ILC2s. Single-cell RNA sequencing (scRNA-seq) confirmed ASCs as a fibroblast-like subset enriched in pathways involved in extracellular matrix remodeling, as well as immune sensing and regulation. *In vitro*, ASCs selectively supported ILC2 and Th2 TRM cell proliferation and cytokine production, predominantly via production of TSLP. *In vivo* depletion of ASCs impaired lung ILC2s, Th2 TRM cells, and the induction of helminth-driven type 2 immunity, in part via ASC-derived IL-33. Together, these data characterize ASCs as a stromal subset that resides in anatomically conserved perivascular niches and demonstrate the importance of ASCs for lung type 2 immune responses.

RESULTS

ILC2s Localize to Adventitial Cuffs

To determine the tissue localization of ILC2s, we imaged IL-5 reporter mice (*Il5-cre*; R26-CAG-RFP, Figure S1A) (Molofsky et al., 2013; Nussbaum et al., 2013). The IL-5-lineage-tracker was both sensitive and specific; ~90% of tissue ILC2s were lineage marked by RFP, ILC2s constituted ~90% of RFP$^+$ cells, and T cells accounted for the remaining RFP$^+$ events (Figures S1B and S1C). Here, we focused on lung ILC2 niches but confirmed results in multiple additional non-barrier tissues. Lung ILC2s localized to bronchovascular areas, with a particular enrichment around arteries (Figure 1A), and often in proximity to lymphatic vessels (Figure 1B). ILC2s also localized to intermediate-to-large vessels in brain meninges (Figure 1C and Video S1) and perigonadal adipose tissue (GAT; Figure 1D). ILC2s were not within vessel or airway lumens (Figure 1E) and instead resided in perivascular adventitial cuff spaces. Lung adventitial cuffs expressed structural Col1A1 but lacked basement-membrane-associated ColIV and were internally bounded by smooth muscle actin (SMA)-positive sheaths (Figures 1F and S1D). Although cuffs accounted for a small fraction of the tissue volume, ~80% of the total ILC2s from lung and brain meninges resided in adventitial cuffs, with slightly lower frequencies in GAT (Figure 1G). When lung pleural surfaces were excluded, >95% of lung ILC2s were in adventitial cuffs, whereas T cells (CD3e$^+$) and DCs were present in both cuff and parenchymal locations, and alveolar macrophages were exclusively present in the lung alveolar parenchyma (Figure 1H). ILC2s were an enriched population within resting lung cuffs, accounting for ~30–50% of non-B lymphocytes, as opposed to 1%–2% in the total lung. ILC2s were similarly distributed in multiple non-barrier tissues including the pancreas (Video S2), mesenteric adipose tissue (MAT), liver, spleen, and uterus, as were rare IL-5$^+$ Th2 TRM cells (Figure S1E). CCL19, a chemokine involved in CCR7-dependent immune cell trafficking to lymph nodes, also labeled lung cuff portions proximal to ILC2s (Figure S1F).

We also examined ILC2 localization in epithelial tissues and serosal body-cavity sites. As expected, GI ILC2s localized to the lamina propria in adult mice (Figures S2A and S2B). Skin ILC2s localized to epithelial areas in proximity to hair follicles (Figure S2C). In SLOs (lymph nodes and Peyer's patches), rare ILC2s localized to capsular, interfollicular, and medullary regions (Figures S2D and S2E). In body cavities (lung pleura, peritoneal membrane, and heart pericardium), ILC2s localized with the mesothelial lining (Figures S2F–S2I). These data indicate that ILC2s reside in perivascular cuff niches, although additional epithelial, nodal, and mesothelial ILC2 tissue niches exist at unique micro-anatomic boundary sites and are consistent with recent evidence describing ILC2 heterogeneity both between and within tissues (Ricardo-Gonzalez et al., 2018). Here, we focused on the ILC2 adventitial cuff niche that was present in virtually all tissues examined.

ILC2s Localize with Subsets of Dendritic Cells and Regulatory T Cells

Next, we identified the immune cells that were proximal to adventitial ILC2s. Lung ILC2s localized with CD11c$^+$MHCII$^+$ myeloid cells, consistent with a DC identity (Figure 2A), as did ILC2s in the liver, kidney, and other tissues (Figures 2B, 2C, and S3A); 80%–90% of ILC2s were in proximity to at least one DC (<1 μm surface to surface), a degree of localization similar to that of lung Treg cells and DCs, and well above DC association with T cells as a whole (~20%; Figure 2D). We found that ~35% of lung DCs were CD301b$^+$ cDC2s expressing CD11c, MHCII, CD11b, CD301b (MGL2), and IL1RL1 (IL-33R, ST2), a subset associated with initiation of type 2 immunity (Durai and Murphy, 2016; Kumamoto et al., 2013) (Figure 2E). ILC2s in multiple tissues co-localized with CD11b$^+$CD301b$^+$ DCs (Figures 2F–2H), including in the lung, where we found a significant enrichment of CD11b$^+$ DCs co-localized with ILC2 (Figure 2I). These findings suggest that previously described ILC2-cDC2 interactions (Halim et al., 2014; 2016) might also occur in adventitial perivascular niches.

IL-33-Expressing Adventitial Stromal Cells Localize with ILC2s

To determine which non-hematopoietic cells are positioned to locally regulate ILC2s, we first used a reporter that marks fibroblast-like stromal cells with a nuclear-localized green fluorescent protein (GFP) (PDGFRα^{GFP}). We visualized a lung GFP$^{low/dim}$ subset (~20% of GFP$^+$ cells) that localized to adventitial cuffs and was distinct from the GFP$^{hi/bright}$ subset in the alveolar parenchyma (Figures 3A–3C). Here, we refer to these GFP^{low} cells as adventitial stromal cells (ASCs), although related stromal subsets from diverse tissues have been called adventitial fibroblasts

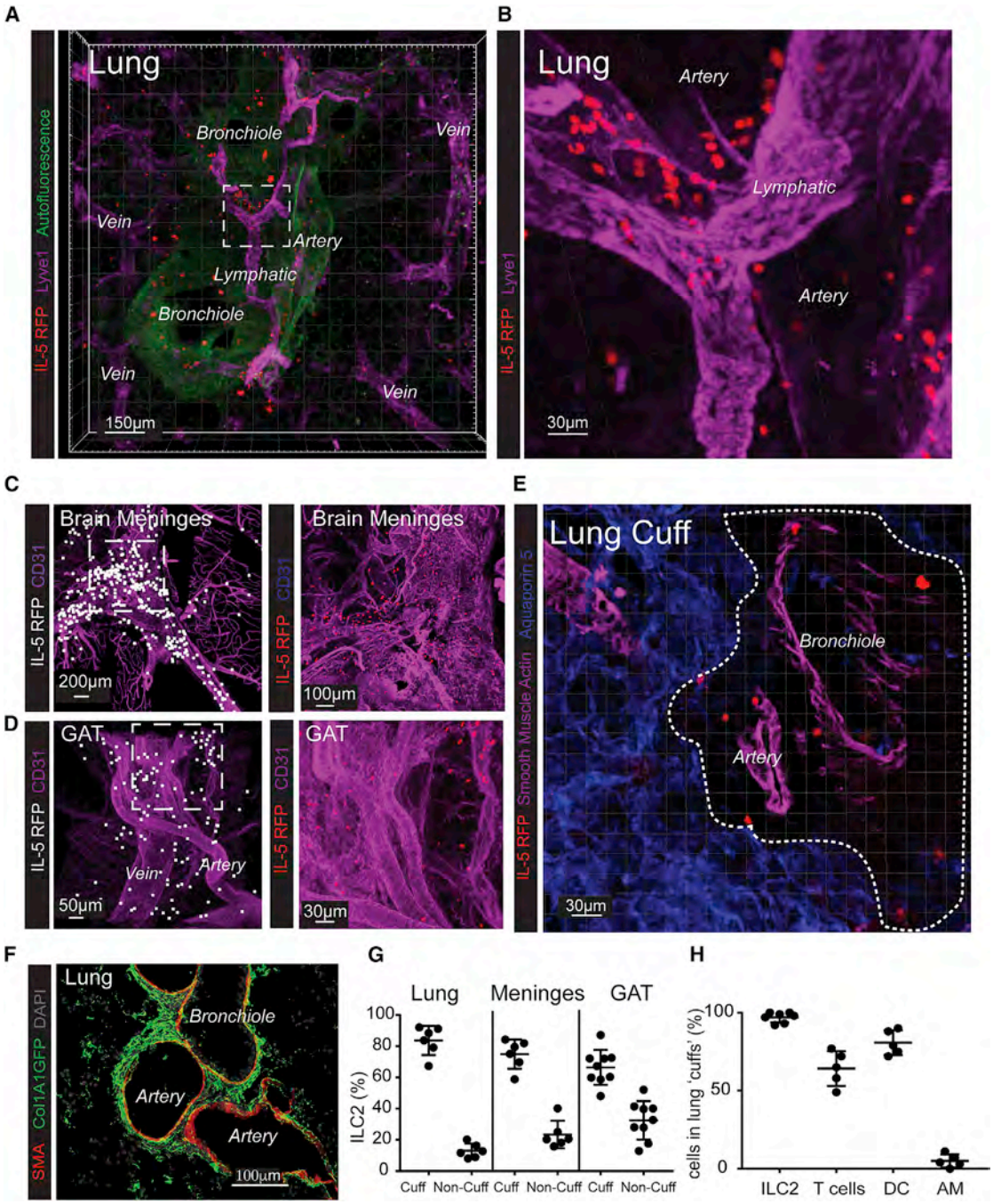

Figure 1. ILC2s Localize to Adventitial Cuffs in Multiple Organs

(A and B) 3D rendering (A) with zoomed-in image (B) of a 200-μm-thick lung slice with IL-5$^+$ ILC2s (RFP), bronchioles (autofluor$^+$Lyve$^-$), arteries (Lyve1^{dim+}, Autofluor$^+$, bronchiole-adjacent), veins (Lyve1^{dim+}, Autofluor$^+$, non-bronchiole-adjacent), and lymphatics (Lyve1$^{bright+}$, Autofluor$^-$) visualized.

(C and D) IL-5 RFP$^+$ ILC2s and CD31$^+$ vessels visualized in (C) brain meninges and (D) perigonadal adipose tissue (GAT).

(E and F) IL-5 RFP$^+$ ILC2s visualized in the lung adventitial cuff, highlighted by a lack of (E) Aquaporin 5 and SMA and the presence of (F) Col1A1-rich cuff regions surrounding bronchioles and arteries.

(G) 3D image quantification of IL-5 RFP$^+$ ILC2s localized within the cuff volume, calculated via automatic surfacing (lungs), or found within 40 μm of SMA$^+$ vasculature (meninges, GAT).

(H) Percentage of cells in lung cuffs: ILC2s (IL-5 RFP$^+$), T cells (CD3ε$^+$), DCs (CD11c$^+$MHCII$^+$ co-positive), and alveolar macrophages (AMs; CD11c$^+$MHCII$^-$). Analysis in (G) included lung cuff, parenchyma, and pleural regions, whereas (H) excluded pleura.

Images are representative of (A–E) 3 or more mice or (F) 2 mice. Data points in (G) and (H) represent averages of individual mice, and n ≥ 5 animals with ≥55 cells of each type were analyzed per mouse. Error bars represent means ± standard deviation. See also Figures S1–S3 and Videos S1 and S2.

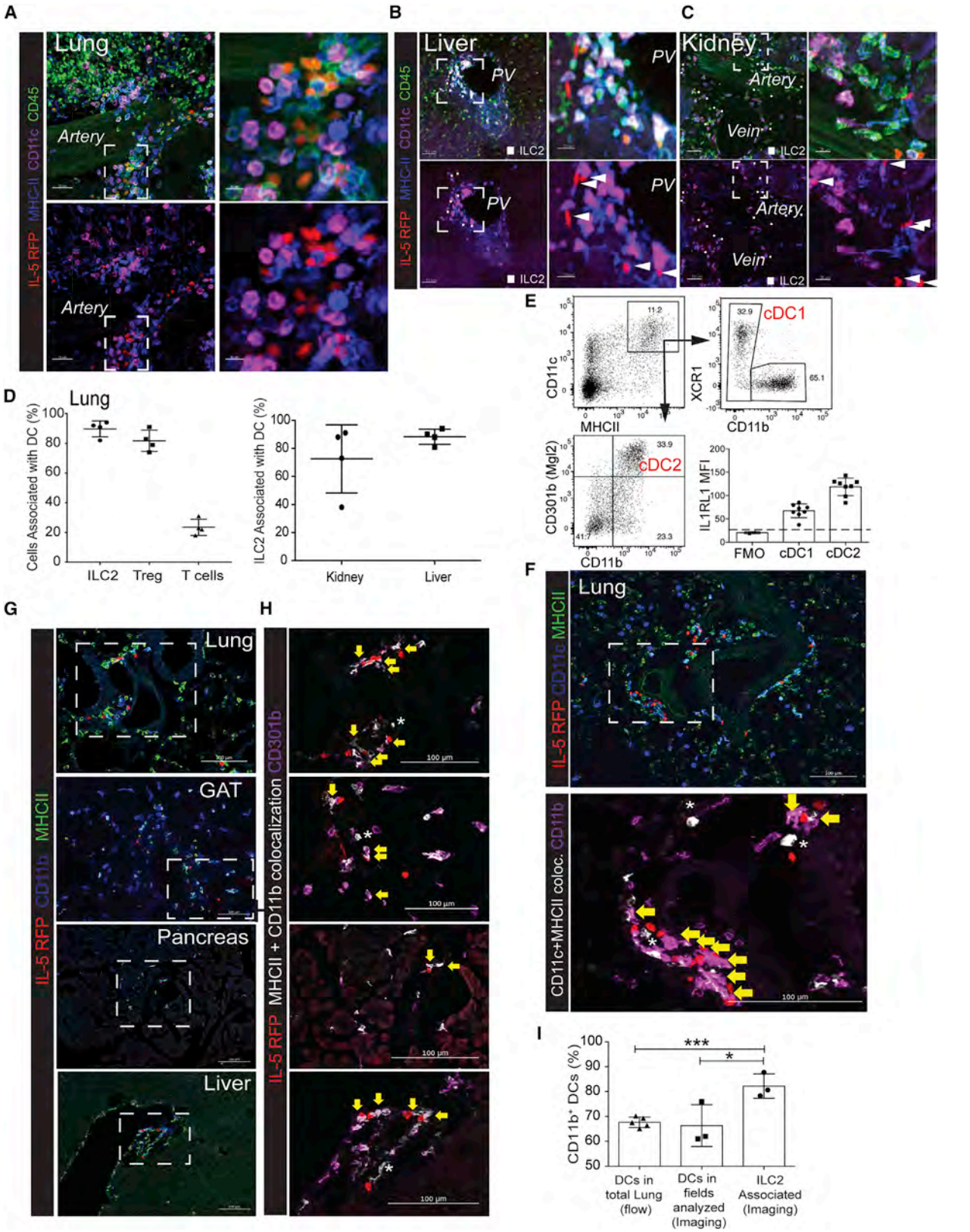

(legend on next page)

(AFs), mesenchymal stromal cells or mesenchymal stem cells (MSCs), fibro-adipogenic progenitors (FAPs), and adipocyte precursors (APs) (Corselli et al., 2012; Sitnik et al., 2016). Using 3D imaging with surfacing, we found that virtually all ILC2s resided in closer proximity to ASCs than to other cuff components, such as smooth muscle cells and blood endothelial cells (Figures 3E and 3F). A subset of ILC2s were also in proximity to the lymphatic endothelium (Figures 3E and 3F).

Next, we determined whether ASCs express signals known to support ILC2 function. First, we examined IL-33, a nuclear-localized IL-1-family cytokine that is released with cell death or stretch and activates ILC2s in cooperation with other tissue-derived signals (e.g., IL-7 and TSLP) (Cayrol and Girard, 2018; Molofsky et al., 2015a). A subset of lung GFP^{low} ASCs (~60%) stained with nuclear IL-33 protein, whereas lung GFP^{hi} parenchymal stroma did not (Figures 3A–3D). Lung ILC2s preferentially localized to the IL-33$^+$ ASC subset, frequently with two or more IL-33$^+$ ASCs in contact with a single ILC2 (Figures 3G and S3C and Video S3), and we had similar findings in the liver, pancreas, and adipose tissue (Figures S3D and S3E and Video S4). Consistent with previous work (Halim et al., 2018; Molofsky et al., 2015b), Treg cell subset(s) from several tissues also localized to ILC2s and DC subsets and to IL-33$^+$ ASCs (Figures S3E–S3G). Lung ASCs did not express detectable IL-7 (IL-7GFP), a signal required for ILC development and optimal lung Th2 TRM cell maintenance (Shinoda et al., 2016), although subset(s) of lung lymphatic cells were IL-7GFP$^+$ (Figures 3H and 3I; Miller et al., 2013; Shinoda et al., 2016). These data suggest that cuff ILC2s intimately associate with IL-33$^+$ ASCs, raising the possibility that ASCs provide IL-33 or other signals that locally regulate ILC2s.

In mice, lung ILC2s expand in the first 2 weeks of life, a postnatal period associated with alveolar and vascular growth and activated lung ILC2s and type 2 immunity (Figure 3J) (de Kleer et al., 2016; Saluzzo et al., 2017). Recent data also indicate that ASC-like stromal cells can promote terminal differentiation of mesenteric ILC precursors to mature ILC2s (Koga et al., 2018). As such, we examined ILC2 localization during early postnatal development. We found that by postnatal day 2 (P2), rare IL-5$^+$ ILC2 were already in close proximity to ASCs in developing lung cuffs, a relationship that was maintained during the next 2 weeks of ILC2 expansion (Figures 3K–3N and S3H). In the liver and small intestine, we identified ILC2s that also associated with IL-33$^+$ stromal cells (Figures S3I–S3K). These data indicate that postnatally expanding ILC2s localize with IL-33-expressing stromal cells, often in adventitial cuff structures, and suggest that the distribution of ILC2s begins early in life.

IL-33mcherry Identifies ASCs in Multiple Tissues

To better characterize the cellular sources of IL-33 within the ILC2 niche, we used IL-33-H2B-mcherry reporter mice (Figure S4A) (Vainchtein et al., 2018). PDGFRαGFP^{low} ASCs preferentially expressed Sca1 (Ly6A) and Gp38 (podoplanin) and ~60% expressed IL-33mcherry (Figure 4A), consistent with IL-33 protein expression (Figures 3A–3D). ASCs were the most abundant IL-33$^+$ cell type in many tissues (Figures 4B and 4C), and IL-33$^+$ ASCs were always a subset of total PDGFRαGFP$^+$ stroma (Figure S4D). However, other lung cells expressed both IL-33mcherry$^+$ and *Il33* transcript, including epithelial (EpCAM$^+$), endothelial (CD31$^+$), and other stromal (EpCAM$^-$CD31$^-$Sca1$^-$) subsets (Figures S4B and S4C). Small numbers of alveolar macrophages were dimly positive for IL-33mcherry, whereas other hematopoietic cells examined were negative in naive lung, peritoneal fluid, and skin (data not shown). Imaging confirmed that IL-33mcherry$^+$ ASCs expressed Sca1 and were the primary IL-33$^+$ cell type in adventitial cuffs of multiple tissues (Figures 4D–4F and S4E–S4H). Other IL-33 sources were also confirmed, including lung epithelial type 2 pneumocytes (AT2), lymph node stromal cells, and endothelial cell subset(s) in lung, liver, and adipose tissues (Figures 4C–4F and data not shown). These data demonstrate that ASCs are a conserved IL-33-expressing stromal subset in adventitial niches in proximity to ILC2s, although additional IL-33-expressing cell types are present in a tissue- and niche-dependent manner (Pichery et al., 2012).

ASCs Are a Molecularly Distinct Stromal Subset Associated with Matrix Remodeling and Inflammatory Response

To gain an unbiased insight into the molecular identity of ASCs, we performed droplet-based scRNA-seq. In sorted lung IL-33mcherry$^+$ cells from pooled mice, we identified four *Il33*-expressing subsets, consistent with our flow-cytometry and imaging data. These were epithelial AT2s (cluster 0), mesenchymal ASCs (cluster 2), mesothelial cells (serosal lining, cluster 3), and endothelial cell subsets (cluster 4) (Figures 5A–C). ASCs (cluster 2) expressed high amounts of *Pdgfra* and *Col1a1* and were enriched with expression of several cytokines (*Tslp*, *Il6*, and *Csf1*), chemokines (*Ccl11*, *Ccl2*, *Ccl7*, *Cxcl12*, and *Ccl19*), growth factors (*Igf1* and *Igf2*), and cytokine receptors (*Ifngr1*, *Il11ra1*, and *Il1r1*) (Figure 5D). Several transcription factors (*Prxx1*, *Prxx2*, and *Klf4*) and nuclear receptors (*Ar*, *Nr4a1*, *Nr4a2*, *Nr4a3*, and *Rora*) were also enriched (Figures 5D and S5A and Table S1). IL-33mcherry$^+$ ASCs were also marked by expression of multiple early-response genes and markers of NF-κB pathway activation, including *Nr4a1*, *Nr4a2*, *Nr4a3*, *Fos*, *Junb*, *Egr1*, *Nfkbia*, *Nfkbiz*, and *Zfp36* (Figure 5D and

Figure 2. ILC2s Are Associated with CD11b$^+$ Dendritic Cells at Cuff Sites

(A–C) 3D rendering with zoom of 200 μm projections from (A) lung, (B) liver, or (C) kidney highlights IL-5RFP$^+$ ILC2 and CD11c$^+$MHCII$^+$ myeloid cells, most consistent with DCs.

(D) Image analysis of 3D thick sections from lung, liver, and kidney for the indicated populations; association is defined as <900 nm between the nearest ILC2 and DC surface vertices.

(E) Flow-cytometry analysis of lung DC subsets.

(F–I) 2D thin-cut images with a zoomed-in view of ILC2 localization (yellow arrows) with (F) CD11b$^+$ DCs or (G and H) CD301b$^+$CD11b$^+$ DCs from indicated tissues and (I) quantification of co-localization. Occasional CD11b$^-$ DCs (F) or CD301b-neg DCs (H) are indicated with stars.

Images in (A)–(C) and (E)–(H) are representative of three or more mice. Data points in (D) and (I) represent averages of individual mice (n = 3 or 4 with >25 cells analyzed per animal). *p < 0.05; ***p < 0.001. Error bars represent means ± standard deviation. See also Figure S3.

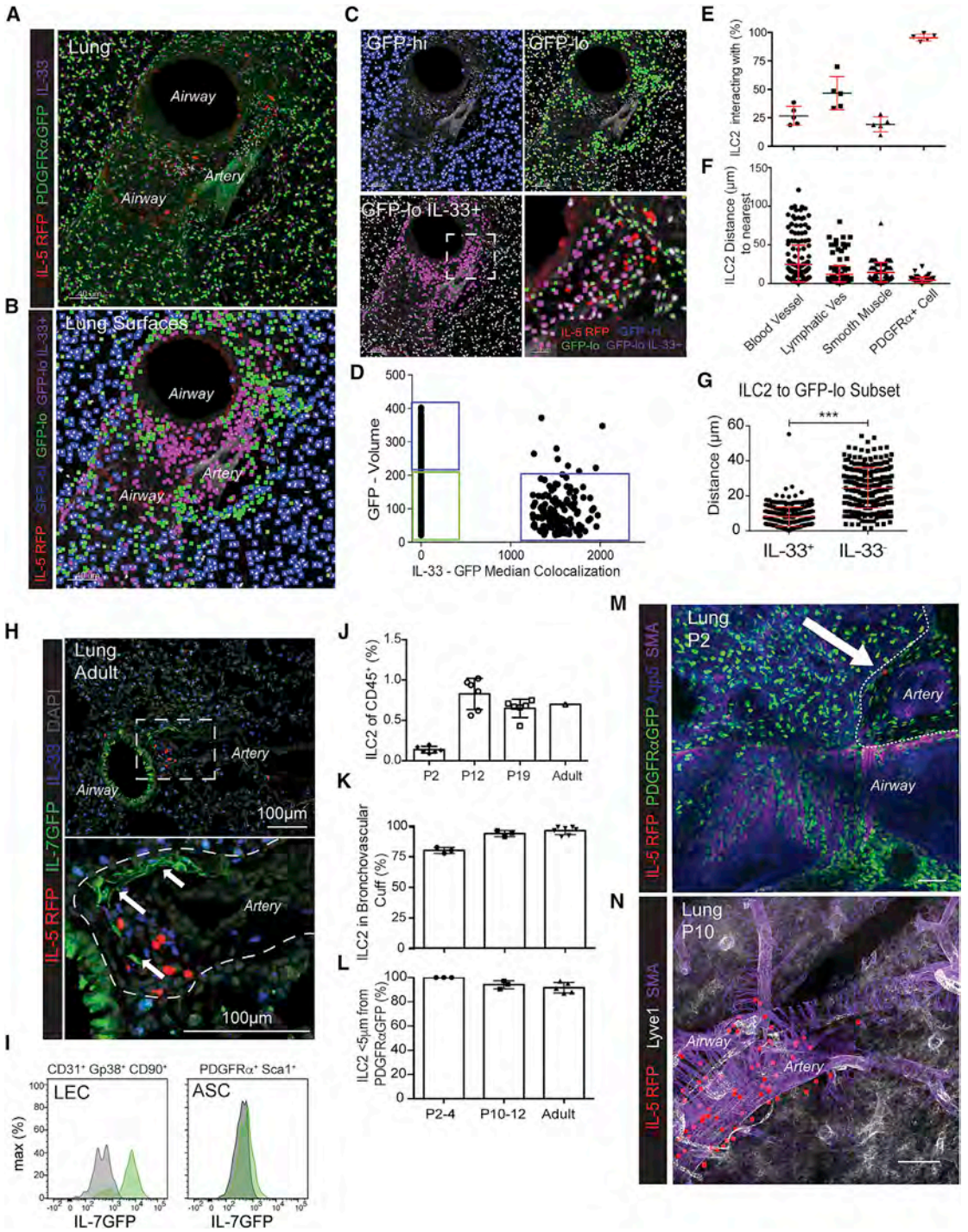

Figure 3. ILC2s Localize with Adventitial Stromal Cells Expressing IL-33

(A) 3D rendering with zoom of a 200-μm-thick projection from a lung-airway-artery region.

(B–D) PDGFRαGFP^{+} stromal cells were surfaced and binned with GFP and IL-33 median co-localization into 3 groups: PDGFRαGFP^{hi}, IL-33^{-} parenchymal stroma (blue), GFP^{low} IL-33^{-} cuff ASCs (green), and GFP^{low} IL-33^{+} ASCs (magenta).

(E–G) Quantification of (E) the percentage of ILC2s (IL-5 RFP^{+}) less than 5 μm apart from blood vessels (Lyve1^{+}SMA-proximal), lymphatic vessels (Lyve1^{+}SMA^{-}), smooth muscle (SMA^{+}), or PDGFRα^{+} stroma (GFP^{+}); (F) the distance from ILC2s (IL-5 RFP^{+}) to the nearest cell type; and (G) the distance from ILC2s to the nearest PDGFRαGFP^{low} ASC subset (IL-33^{+} versus IL-33^{-}).

(H) Lung 2D section highlighting ILC2 (IL-5RFP^{+}) and IL-7GFP^{+} lymphatics. Note green autofluorescence in airways.

(I) Flow-cytometry analysis of IL-7GFP and wild-type (WT) controls for the indicated populations.

(J) Flow-cytometry analysis of ILC2s (Lin^{-}Thy1^{+}Gata3^{hi}) in developing WT lungs at indicated postnatal days (P2, P12, P19, and >8-week-old adults).

(legend continued on next page)

Table S1). These findings suggest that lung ASCs have potential roles in immune responses, wherein they express genes implicated in the regulation of type 2 immunity, including *Il33*, *Tslp*, and *Ccl11* (eotaxin-1).

To identify unique molecular markers of IL-33$^+$ ASCs versus other IL-33$^-$ stromal subsets, we compared ASCs with all non-hematopoietic cells (CD45$^-$) in the lung (Figure 5E). Cluster 5 cells were enriched with genes encoding Sca1 (*Ly6A*), Gp38 (*Pdpn*), and IL-33, consistent with an ASC identity. In addition, this subset expressed relatively elevated amounts of collagens and chemokines and was enriched with Gene Ontology (GO) terms associated with extracellular matrix remodeling and immune response (Figures 5F and 5G, Table S1, and Figure S5B). Cluster 5 ASCs did not express detectable *Il7* (Table S1), although *Il7* was detectable in a lymphatic endothelial sub-cluster, consistent with the IL-7GFP reporter results (Figures 3H and 3I). ASCs were distinct from putative smooth muscle cells (cluster 17) or pericytes (cluster 14), which lacked *Il33* and *Col1a1* (Table S1).

We identified a similar stromal subset in gonadal adipose tissue (GAT), where IL-33mcherry$^+$ cells clustered into four groups (Figures S5C and S5D), including mesothelial cells (cluster 1; expressing *Wt1* and *Msln*) and three stromal subsets (clusters 0, 2, and 3; all expressing *Pdgfra* and *Col1a1*). The largest stromal subset (cluster 0) was enriched with *Ly6a*, *Cd34*, *Pi16*, *Ccl11*, and *Cxcl1* and was similar to lung ASCs (Figures S5D–S5F). These data indicate that lung and adipose tissue IL-33mcherry$^+$ ASCs are transcriptionally related subsets. Similar ASC-like populations expressing transcripts for CD34, Ly6A, TSLP, and IL-33 were identified in scRNA-seq datasets from multiple tissues (Han et al., 2018), suggesting that ASCs have conserved functions that include the regulation of local immune responses.

ASCs Produce TSLP to Support ILC2s

To test whether lung ASCs were sufficient to support ILC2s *in vitro*, we sorted lung ILC2s and co-cultured them with subsets of lung stromal cells. *In vitro*, ILC2s require STAT5-activating cytokine supplement (i.e., IL-2, IL-7, and TSLP) for survival and proliferation, and IL-33 synergizes with these signals to provide increased ILC2 activation and proliferation. Surprisingly, bulk lung stroma was sufficient to maintain ILC2s in the absence of exogenous cytokines (Figure 6A). We found that sorted ASCs (PDGFRα^+Sca1$^+$) and parenchymal-enriched stromal cells (PDGFRα^+Sca1$^-$) formed similar monolayers and stabilized at similar cell densities (Figures S6A and S6B), yet ASC co-cultures yielded ~4-fold more ILC2s (Figure 6B). *In vivo*, tissue ILC2s produce constitutive IL-5 and variable IL-13 (Molofsky et al., 2013; Nussbaum et al., 2013; Van Dyken et al., 2014). Similarly, *in vitro* ASCs supported low amounts of ILC2 IL-5 and IL-13 production (Figures 6C and 6D).

ASC-conditioned media (ASC-CM) was also sufficient to support ILC2s in a dose-dependent manner (Figures 6E and 6F), suggesting the presence of ASC-secreted factor(s). ASCs expressed *Tslp* transcript (Figure S6C), and ASC-CM contained TSLP protein, but not IL-7 or IL-33 (Figures 6G and S6E and data not shown). Blockade of TSLP impaired the ability of ASC-CM and ASCs to support ILC2s and their proliferation (Figures 6H and S6D–S6F), whereas TSLP alone was sufficient to support ILC2s (Figure 6I). ASCs and ASC-CM also supported IL-5$^+$ Th2 cells (CD4$^+$CD44$^+$IL-5RFP$^+$; Figures 6J and 6K) in a TSLP-dependent manner. In contrast, other lung CD4$^+$ T cell naive or memory subsets were not supported by ASCs. Although ASCs did not release detectable IL-33 protein under the *in vitro* conditions tested, ASC-derived IL-33 was bioactive and conferred additional support to ILC2s after ASC lysis (Figure 6L). We concluded that ASCs can support both ILC2 and Th2 TRM cells via TSLP production, consistent with the ability of purified TSLP and related STAT5-activating cytokines (i.e., IL-2 and IL-7) to support these type 2 lymphocytes (Halim et al., 2012; Mohapatra et al., 2016). However, additional ASC-derived signal(s) might also contribute to ILC2 and Th2 TRM cell regulation.

ILC2s and IL-13 Promote ASC IL-33 Expression

Next, we tested whether ILC2-derived signals reciprocally regulate ASCs. *In vitro*, both ILC2s and IL-5$^+$ Th2s, but not other lung CD4$^+$ T cells, promoted increased ASC IL-33mcherry expression (Figures 6M, 6N, and S6I). These type 2 lymphocytes expressed IL-13 after activation, and ASCs expressed both components of the IL-13 receptor (Figures S6G and S6H). IL-13 treatment significantly increased ASC IL-33mcherry expression, in contrast to several other cytokines and signals for which ASCs expressed receptors and that have been reported to increase IL-33 production (IL-1β, PDGF-BB, or IL-17A + TNFα; Figure S6J). PDGF-BB increased ASC numbers (~2.3-fold, not shown) and IL-1β and IL-17A + TNFα promoted ASC TSLP production (Figure S6K), indicating that these compounds are bioactive and most likely regulate additional aspects of ASC biology. *In vivo*, repetitive intranasal administration of IL-13 or IL-4 increased both ASC and epithelial cell IL-33mcherry expression and promoted lung eosinophil accumulation (Figure S6L and data not shown).

Type 2 Immune Challenges Drive ILC2 and Th2 Cell Expansion in Cuffs

To examine the relationship of ILC2s and Th2 cells with the adventitial cuff during type 2 inflammation, we determined the localization of these type 2 lymphocytes after helminth infection. *N. brasiliensis* is a model helminth that traffics from skin to lung and is cleared through the intestine by post-infection (PI) day 7 (Molofsky et al., 2013; Nussbaum et al., 2013). IL-5$^+$ Th2 TRM cells are rare in naive lungs but expand along with ILC2s and persist for extended periods after helminth infection (Nussbaum et al., 2013; Van Dyken et al., 2016). At PI week 4, lung IL-5$^+$ cells were a mix of ILC2s and Th2 TRM cells that localized predominantly to adventitial cuffs in proximity to IL-33$^+$ ASCs (Figures 6O, S6M, and S6N). The percentage of ILC2s in adventitial cuffs modestly changed from >95% in naive mice to ~75%

(K and L) 3D imaging of 200-μm-thick section from pups at the indicated ages shows (K) the percentage of ILC2s in the lung cuff and (L) localization between ILC2 and PDGFRαGFP$^+$ stroma.

(M and N) 3D rendering of (M) 25 μm or (N) 52 μm volume from lungs at the indicated postnatal ages highlights ILC2 localization.

Data points represent (E and J–L) the average per mouse or (F) the aggregation of five individual mice (n = 237). Images, surfaces, or flow-cytometry analysis in (A)–(D), (H), (I), (M), and (N) represent 3 or more mice. ***p < 0.001. Error bars represent means ± standard deviation. See also Figure S3 and Videos S3 and S4.

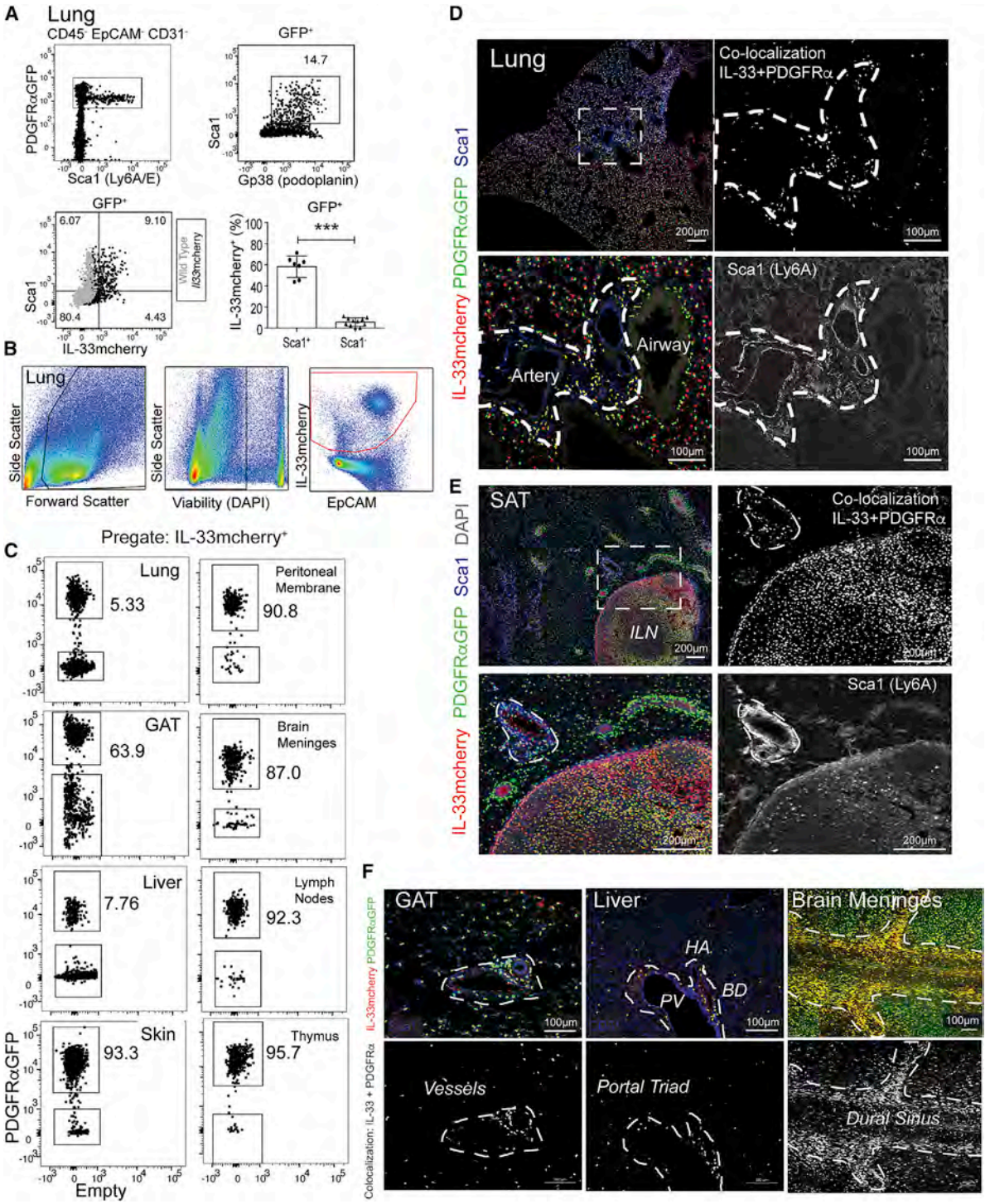

Figure 4. ASCs Express IL-33mcherry, Sca1, and Gp38 and Are Widely Distributed in Tissues

(A–C) Flow-cytometry plots and quantification from (A) lung of PDGFRαGFP⁺IL-33mcherry mice (black) or WT gating controls (gray) or (B and C) indicated tissues, including pre-gating strategy.

(D–F) 2D thin-cut images with zooms from (D) lung, (E) subcutaneous adipose tissue (SAT) with inguinal lymph node (ILN), or (F) gonadal adipose tissue (GAT), liver, and brain meninges; antibody stains are indicated, and PDGFRαGFP-IL-33mcherry co-localization is highlighted (white).

Flow-cytometry plots and images are representative of 3 or more mice. ***$p < 0.001$. Error bars represent means ± standard deviation. See also Figure S4.

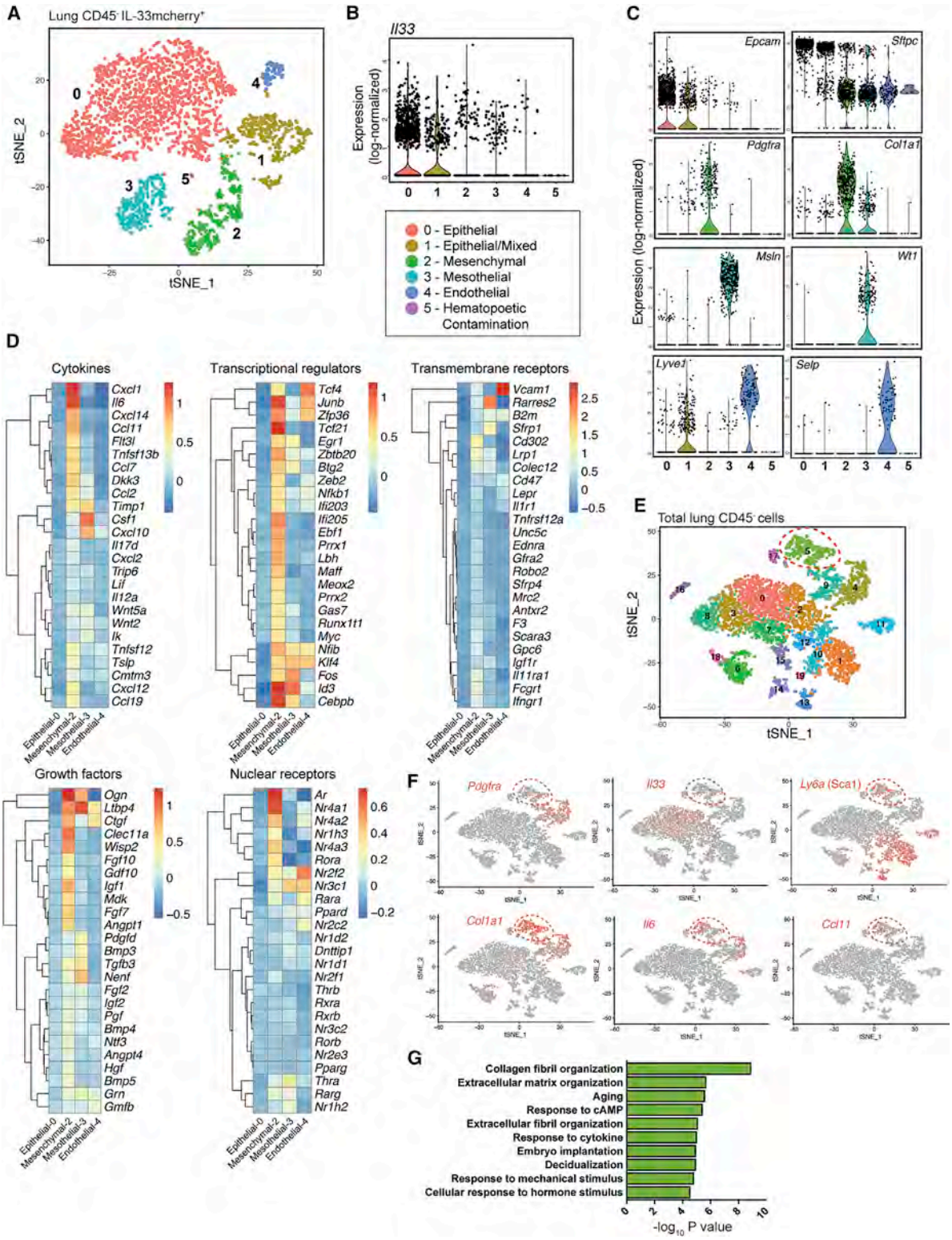

Figure 5. ASCs Are a Distinct IL-33-Expressing Fibroblast-like Subset Expressing Genes Associated with Matrix Remodeling and Inflammation

(A) Unsupervised clustering analysis of scRNA-seq on IL-33mcherry^{+}CD45^{-} cells from naive lung visualized with t-SNE. Each dot indicates an individual cell (total cell number: 3,584). A mixed subset comprising apparent epithelial with endothelial cell doublets (cluster 1) and a small hematopoietic contaminating subset (cluster 5) were identified and not analyzed further.

(legend continued on next page)

after *N. brasiliensis* infection, similarly to that of Th2 TRM cells (Figure 6P). ILC2s and Th2 cells showed similar cuff localization in a papain model of type 2 lung inflammation (Figure 6Q) and after systemic IL-33 injections, which expanded ILC2s in cuff structures in multiple tissues, including liver, spleen, adipose tissue, and lung (Figures 6O and S6O and data not shown). We conclude, in the tissues tested, that during type 2 inflammatory challenges, ILC2s and Th2 TRM cells are primarily localized to adventitial cuff niches and in proximity to ASCs, although small subset(s) of type 2 lymphocytes expand into parenchymal niches.

Type 2 Inflammation Promotes IL-33$^+$ ASC Expansion Dependent on ILC2s

Concurrent with ILC2 and Th2 cell expansion, we found increased IL-33mcherry expression in ASCs (PDGFRαGFP^{lo} Sca1$^+$) and increased frequency and IL-33 expression in GFP^{low}Gp38$^+$Sca1$^-$ stromal cells, both localized predominantly to adventitial cuffs after helminth infection (Figures 6R, 6S, S6P, and S6Q). scRNA-seq indicated that the four IL-33mcherry$^+$ populations identified in naive lungs were also present at PI day 30, although both ASCs and lymphatic endothelial cells relatively increased (Figure S5G). Modest transcriptional changes, including decreased expression of several collagen- and matrix-related genes (*Col1a1*, *Col1a2*, and *Dpt1*), in IL-33mcherry$^+$ ASCs were noted after infection (Table S1). Loss of ILC2s (*Il5-cre*; R26-DTA; ~80%–90% deletion) impaired the helminth-driven expansion of IL-33$^+$PDGFRαGFP^{low} ASCs (Figures 6T and S6R–S6U). These results were supported by decreased cuff-localized IL-33 in ILC2 deleter mice, analyzed by quantitative imaging (controls, 3.6×10^5 per mm^3 ± 6.8×10^4; ILC2-deficient, 1.3×10^5 per mm^3 ± 3.7×10^4; n = 2 per group, PI day 14). These findings suggest that ASCs dynamically expand and increase IL-33 expression after type 2 inflammation, and ILC2s promote this niche remodeling.

ASCs Support Helminth-Driven Induction of ILC2s and Type 2 Immunity

Next, we tested whether ASCs support type 2 inflammation *in vivo*. scRNA-seq identified a number of potential markers expressed in ASCs (e.g., *Col1a1*, *Pdgfra*, and *Pdgfrb*), but many of these were broadly expressed during development or lacked specificity for ASCs. The hedgehog family effector Gli1 was enriched in our dataset of IL-33mcherry$^+$ ASCs, and previous work has defined Gli1 expression in similar lung adventitial stroma (Kramann et al., 2015). We confirmed that ASCs co-expressed Gli1, Sca1, and Gp38 in bronchovascular cuffs and several other perivascular regions (Kramann et al., 2015), accounting for over 80% of total lung Gli1$^+$ cells at rest and after type 2 stimuli (Figures 7A, 7D, and S7A–S7D).

To deplete lung ASCs, we used tamoxifen-inducible expression of Diphtheria toxin-α in Gli1-expressing cells (*Gli1-cre*ERT2; R26-DTA) and observed an overall deletion efficiency ranging from 50–75% (Figures 7B and 7C). We found no differential impact on mouse viability in the time frame analyzed, as previously reported (Kramann et al., 2015). In naive mice, ILC2s were not reduced after Gli1$^+$ cell deletion (Figures S7E and S7F), potentially consistent with the slow turnover of adult tissue ILC2s (Nussbaum et al., 2013). However, *N. brasiliensis* infection with concurrent depletion of Gli1$^+$ cells reduced lung IL-33$^+$ ASCs, as expected, and the accumulation of adventitial hematopoietic cells (Figures 7E–7G). Flow-cytometry analysis showed preserved numbers of blood and bone marrow ILC2s (Figure 7H) but reduced accumulation of lung ILC2s, Th2 cells, eosinophils, and Gata3^{hi} type-2-skewed Treg cells (Figures 7I–7L, S7G, and S7H; PI days 12–14), as well as preserved lung CD8$^+$ T cell numbers (Figure S7I) and lymph node CD4$^+$ and CD8$^+$ T cells (data not shown). These data indicate that ASCs are required for optimal accumulation of lung ILC2s, Th2 TRM cells, and helminth-driven type 2 immune responses.

IL-33 and TSLP are not required for ILC2 development or tissue residency, although they synergize to promote ILC2 activation at rest and after type 2 immune challenge (Ricardo-Gonzalez et al., 2018; Van Dyken et al., 2014). Therefore, we tested whether ASC-derived IL-33 contributed to allergic inflammation-driven type 2 lymphocyte accumulation and function. First, we treated ASC-deficient or littermate controls with exogenous IL-33 (Molofsky et al., 2015b). In mice deficient in Gli1$^+$ ASCs, we observed a modest reduction in IL-33-driven eosinophil and Gata3^{hi} Treg cell accumulation and a trend toward fewer ILC2s (Figures S7J–S7L), suggesting that exogenous IL-33 was unable to fully bypass the loss of ASCs, which is consistent with a possible role for additional ASC-derived signals (e.g., TSLP). Next, we tested the converse: whether ASC-derived IL-33 contributes to type 2 immune function *in vivo*. We conditionally deleted *Il33* from ASCs and validated loss of IL-33 protein and message (*Gli1-cre*ERT2; *Il33*$^{F/F}$; Figures S7M and S7N). Mice with IL-33-deficient ASCs showed impaired helminth-driven induction of Th2 cells and a trend toward reduced eosinophils and Gata3^{hi} Treg cells (Figures 7M–7P), despite limited expansion of ILC2s in this mixed genetic background (Chen et al., 2015), which is potentially consistent with mouse-strain-dependent variations in ILC2 activation to type 2 challenges (Molofsky et al., 2013; Oboki et al., 2010). However, additional cellular sources of lung IL-33 (Figures 5A and 5B) might also cooperate with ASCs to coordinately promote ILC2 expansion. Together, our data indicate that ASCs are an important potentiator of lung type 2 immune responses, where they promote type 2 lymphocyte expansion and the orchestration of allergic immune responses via both IL-33-dependent and -independent pathways.

(B and C) Violin plots of (B) *Il33* or (C) selected genes used for assigning cluster identity.
(D) Heatmaps of mean expression values of the top 25 genes in ASCs (cluster 2) in the indicated gene category across clusters identified in (A). Data are log transformed. Genes were assigned to categories with Ingenuity Pathway Analysis (IPA).
(E) Unsupervised clustering of aggregated total CD45$^-$ and IL-33$^+$ (mCherry$^+$) cells from naive lung visualized with t-SNE. Each dot indicates an individual cell (total cell number: 5,392).
(F) Gene expression of ASC-associated genes projected onto t-SNE plots.
(G) GO analysis in DAVID of cluster 5 differentially expressed genes.
See also Figure S5 and Table S1.

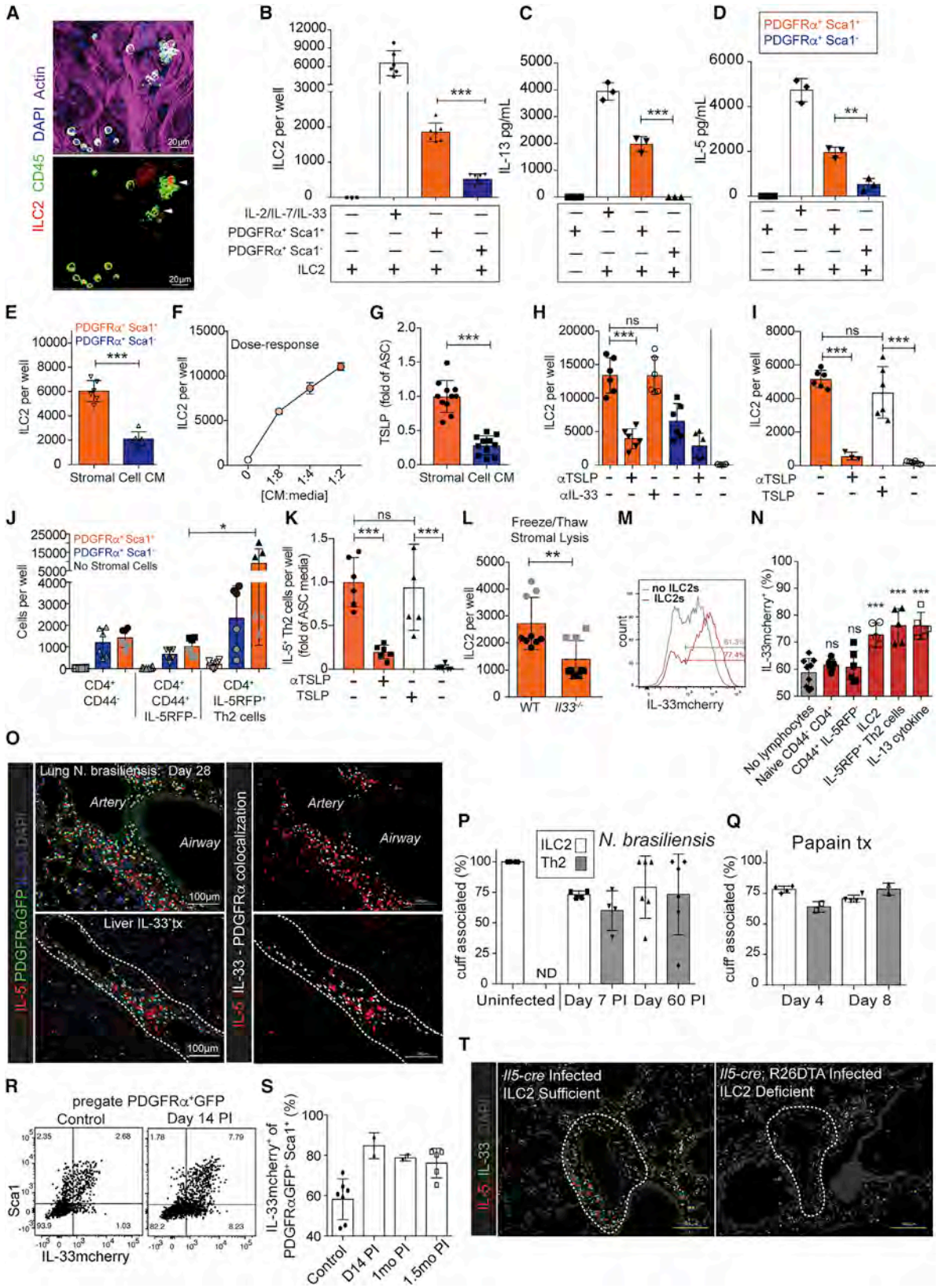

(legend on next page)

DISCUSSION

Here, we have defined a conserved microanatomical niche of ILC2s and demonstrated its role in supporting type 2 immunity after helminth infection. We found that ILC2s predominantly resided in the adventitial cuffs of lung vessels and airways and showed similar cuff localization in the vascular tree of adipose tissue, liver, kidney, spleen, meninges, and pancreas. Within this niche, ILC2s localized with a population of mesenchymal, fibroblast-like ASCs. ASCs are transcriptionally defined by matrix deposition and remodeling functions, but we also identified an immune-related program that included expression of the cytokines IL-33 and TSLP. Lung ASCs were responsive to type-2-lymphocyte-derived signals, including IL-13, and expanded with ILC2s and Th2 TRM cells after helminth infection. After helminth infection, ASCs were partially necessary, and entirely sufficient, to support ILC2 survival, proliferation, and cytokine production. ASCs also supported tissue-resident Th2 cells, establishing ASCs as a niche cell supporting type 2 lymphocytes and the induction of allergic immune responses. ILC2s are long-lived and slowly proliferating cells, and although we found minimal impact of short-term ASC depletion on adult ILC2 numbers, differences in homeostatic maintenance might not be revealed within this time frame. It is also possible that other niche cells provide redundant signals that support ILC2s at rest.

Lung perivascular cuffs were originally defined in models of pulmonary edema as conduits for excess fluid drainage from the alveolar parenchyma to lymphatics. Similar spaces have been identified in humans, and are defined by intermittent compression (e.g., arterial pressure waves), pre-lymphatic fluid flow, the presence of $CD34^+$ fibroblast-like stromal cells, and well-organized collagen fibrils (Benias et al., 2018). Niches for hematopoietic cells often include stromal cells that cooperate with specialized endothelial cells, for example, bone marrow hematopoietic stem cells, lymphocytes in SLOs, and inflammation-induced TLOs. Our work demonstrates that tissue-resident type 2 lymphocytes localize to adventitial niche sites that also include specialized stromal cells (ASCs) and both lymphatic and blood endothelial components, and it further emphasizes that the concept of tissue niches is relevant to understanding the regulation of tissue-resident lymphocytes and the initiation of tissue immune responses.

The potential for immune cell interactions within the cuff raises interesting questions about the regulation of type 2 immunity. A subset of tissue Treg cells are in close proximity to cuff ILC2s and expand in response to IL-33 via both direct and ILC2-dependent effects (Halim et al., 2018; Molofsky et al., 2015b; Panduro et al., 2016), suggesting that ASCs and their IL-33 production might also regulate Treg cell subset(s). We also demonstrated here that cDC2s, previously implicated in the induction of type 2 immune responses, were enriched at cuff sites and localized with ILC2s. Both cDC2 and Treg cell subsets can also respond directly to IL-33 and TSLP to promote their type 2 and/or tissue reparative functions (Kashiwagi et al., 2017; Molofsky et al., 2015a; Panduro et al., 2016; Ziegler, 2012). Further work is needed to understand these intriguing cellular interactions occurring in adventitial spaces.

Key open questions remain regarding the identity of the signals that establish the ILC2 niche during development, the crosstalk between niche immune and stromal cells, and—importantly—to what extent this is a conserved physical location for tissue type 2 immunity in mouse and human. For example, what is the contribution of other components to the ILC2 cuff niche? Microanatomic localization of ILC2 in both cuff- and serosal-boundary spaces closely mirrors that of tissue lymphatics and peripheral nerves. What is the mechanism by which ILC2s and IL-13 feedback to affect ASCs and help shape tissue (re)modeling? ASCs themselves are probably heterogenous and include cells with mesenchymal progenitor capacity (Cano et al., 2017; Kramann et al., 2015; Sitnik et al., 2016) that directly respond to type 2 cytokines (Heredia et al., 2013) and could contribute to niche and tissue remodeling after challenge. What other signals regulate ASC function, including IL-33 and TSLP expression and release? Although ASCs contain bioactive IL-33 protein and upregulate *Il33* message in response to ILC2-derived signals such as IL-13, no IL-33 release was detected

Figure 6. ASCs Produce TSLP to Support ILC2s, whereas ILC2s and IL-13 in Turn Promote ASC Accumulation and IL-33 Expression

(A) Bulk lung stroma was co-cultured with ILC2s for 3 days and imaged with IL-$5RFP^+$ ILC2 clusters indicated.

(B–D) PDGFRα^+Sca1^+ (ASCs, orange) and PDGFRα^+Sca1^- (parenchymal-enriched, blue) stromal cells were cultured with lung ILC2s for 7 days; (B) ILC2s were counted, and (C and D) IL-5 and IL-13 amounts were measured from culture supernatants.

(E–I) Culture media (CM) from ASCs (Sca1^+, orange), control parenchymal-enriched stromal cells (Sca1^-, blue), or fresh culture media (white) were plated with freshly sorted ILC2s for (F) 3 days or (E, H, and I) 5 days with or without the indicated blocking antibodies or TSLP supplementation (10 ng/mL) or (G) assayed for TSLP.

(J and K) Indicated lung T cell subsets sorted from IL-33-treated mice were (J) co-cultured with the stromal cell subsets for 5 days without TCR stimulation or (K) cultured with ASC culture media (orange) or fresh culture media (white) with or without the indicated blocking antibodies or TSLP (10 ng/mL).

(L) ASCs from WT or IL-33-deficient mice were subjected to 3 rounds of freeze-thaw lysis, after which ILC2s were co-cultured for 5 days.

(M and N) IL-33mcherry$^+$ ASCs were cultured for 5 days after confluency with the indicated cells or cytokines (10 ng/mL) and assessed for IL-33mcherry; shown is (M) a representative histogram or (N) the percentage of IL-33mcherry-expressing cells.

(O) Mice were infected with 500 *N. brasiliensis* or treated 3× with 500 ng of IL-33 and examined for the indicated markers.

(P) 200-μm-thick tissue slices were analyzed at the indicated points after *N. brasiliensis* infection or (Q) after papain treatment (3 daily doses), ILC2s (IL-5 RFP^+CD3e^-), Th2 cells (IL-$5RFP^+CD3e^+$); cuff regions (Aqp5^-, bronchovascular associated) were defined, and the association was enumerated.

(R and S) Flow-cytometry analysis of lungs on *N. brasiliensis* post-infection (PI) days is indicated with (R) representative ASC flow-cytometry plots and (S) quantification of ASC IL-33mcherry expression.

(T) 2D thin-cut lung images at PI day 28 from ILC2-deleter (*Il5-cre*; R26-DTA) and control *Il5-cre* mice; IL-5^+ cells and IL-33^+ cells are highlighted.

Data are (A, C, D, F, M, and R) representative or (B, E, G–L, and N) aggregated from 2–3 independent cohorts. Images in (O) and (T) represent two independent experiments. Data in (P), (Q), and (S) were aggregated from 2 independent experiments, and each data point represents 1 mouse. Independent cohorts in (J) and (L) are indicated with black and gray symbols. *$p < 0.05$; **$p < 0.01$; ***$p < 0.001$; ns, not significant. Error bars represent means ± standard deviation. See also Figure S6.

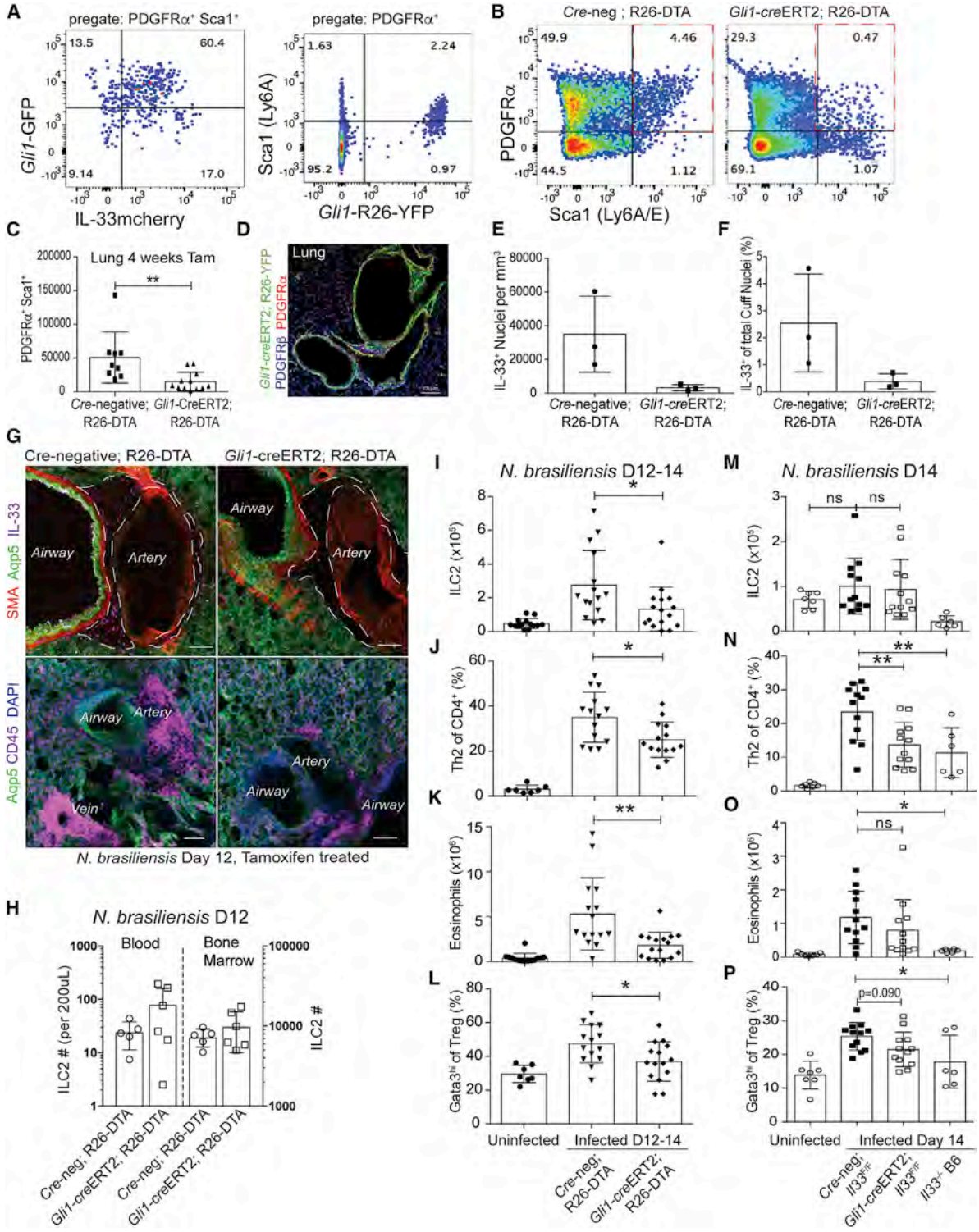

Figure 7. ASCs Support ILC2s and the Induction of Lung Type 2 Inflammation

(A) Flow-cytometry analysis of lungs from *Gli1*-GFP mice (left) or *Gli1-cre*ERT2; R26-YFP tamoxifen-treated lineage trackers (right).

(B and C) Flow cytometry analysis of lungs from *Gli1-cre*ERT2; R26-DTA Cre-negative control mice (tamoxifen treated) (B) with enumeration of ASC depletion (C).

(D) Lung 2D thin-cut image from *Gli1-cre*ERT2; R26-YFP tamoxifen-treated mice.

(E–G) 3D imaging with quantitation of ASC-repleted (*Cre*$^{-}$; R26-DTA) or ASC-depleted (*Gli1-cre*ERT2^{+}; R26-DTA) IL-33^{+} nuclei in adventitial cuff spaces at PI day 12 with *N. brasiliensis*.

(legend continued on next page)

in vitro, suggesting that additional niche components (e.g., cytokines and mechanical stretch) are necessary. In contrast, TSLP was constitutively expressed by ASCs but could be further driven by IL-1β and TNFα + IL-17A, findings that are similar to those in cancer-associated fibroblasts (De Monte et al., 2011). What signals localize ILC2s and Th2s to adventitial niches? Lung ILC2s expand postnatally during a period of development that correlates with the first 3 years of human life, a critical window for the development of allergic asthma in children (Lambrecht and Hammad, 2017). Although ASCs express both TSLP and IL-33, neither of these signals are required for ILC2 or Th2 TRM cell tissue colonization or identity (Ricardo-Gonzalez et al., 2018), suggesting other niche-derived signals might recruit and expand ILC2s (or ILC precursors) and Th2s at these sites. The relationship between ASCs and the stromal cells recently reported to promote fetal-liver-derived ILC2 development remains to be determined (Koga et al., 2018) but, along with our data, raise the possibility that ASCs are involved in ILC2-development and/or postnatal deposition in tissues.

IL-33 and TSLP are both implicated in human studies and multiple mouse models of allergic asthma (Molofsky et al., 2015a). Our data demonstrate that lung ILC2s reside in ASC-rich cuff niches early in development and are distant from epithelial, IL-33-producing type 2 pneumocytes. Although epithelial cells contribute to ILC2 activation and the pathogenesis of allergic lung disease, the contribution of IL-33 and TSLP from mesenchymal sources such as ASCs might also be important. Further, given the close proximity of ILC2s to ASCs in multiple tissues, additional ASC-derived, contact-dependent or secreted, signals are likely to be involved in ILC2 regulation. Recent studies have identified subsets of stromal cells and their IL-33 production in the regulation of tumor-associated macrophages, pancreatic insulin production, and neuronal synapse remodeling (Dalmas et al., 2017; Yang et al., 2016; Vainchtein et al., 2018), suggesting that stromal-immune crosstalk regulates both physiologic and pathologic tissue immunity. Ultimately, a precise anatomic understanding of the regulation of tissue-resident immune cell niche size, composition, and expansion could have profound implications for a variety of diseases, including allergic asthma, fibrosis, diabetes, cancer, neurodevelopmental disorders, and cardiovascular disease.

STAR★METHODS

Detailed methods are provided in the online version of this paper and include the following:

SUPPLEMENTAL INFORMATION

Supplemental Information can be found with the article online at https://doi.org/10.1016/j.immuni.2019.02.002.

ACKNOWLEDGMENTS

We thank the University of California, San Francisco (UCSF) Biological Imaging and Development Core and members Adam Fries and Kyle Marchuk (confocal microscopy and analysis); the UCSF Institute for Human Genetics and members Eunice Wan and Dedeepya Vaka (scRNA-seq); Satoru Joshita and Marco Colonna (IL-33mcherry mice); Dean Sheppard and Tom Arnold (Col1A1GFP mice); Richard M. Locksley and Adrian Erlebacher (comments and discussion); Z.E. Wang (cell sorting); and H.E. Liang (assistance with *N. brasiliensis* stocks). A.B.M. is supported by the National Institute of Diabetes and Digestive and Kidney Diseases (NIDDK, K08DK101604), the National Heart, Lung, and Blood Institute (NLHBI, R56HL142701), the Larry L. Hillblom Foundation, the Sandler Asthma Basic Research Center, the UCSF Department of Laboratory Medicine, and a grant from the UCSF Program for Breakthrough Biomedical Research; S.W.J. is supported by the American Cancer Society post-doctoral fellowship (PF-15-157-01-CSM); and M.W.D. is supported by the Swedish Society for Medical Research and a UCSF Bold & Basic fellowship.

AUTHOR CONTRIBUTIONS

Conceptualization, M.W.D., S.W.J., K.M.C., T.P., A.V.M., and A.B.M.; Methodology, S.W.J., M.W.D., K.M.C., M.F.K., and A.B.M.; Investigation, S.W.J., M.W.D., K.M.C., A.D., S.F., J.F.O.-C., C.W., K.S.Y., K.L., and A.D.T.; Writing – Original Draft, S.W.J., M.W.D., and A.B.M.; Writing – Review & Editing, M.W.D., S.W.J., M.F.K., and A.B.M.; Funding Acquisition, M.W.D., S.W.J., A.V.M., and A.B.M.; Resources, A.B.M.; Data Curation, K.S.Y., K.L., and A.D.T.; Supervision, T.P., A.V.M., and A.B.M.

DECLARATION OF INTERESTS

The authors declare no competing interests.

Received: May 23, 2018
Revised: November 7, 2018
Accepted: February 1, 2019
Published: February 26, 2019

REFERENCES

Benias, P.C., Wells, R.G., Sackey-Aboagye, B., Klavan, H., Reidy, J., Buonocore, D., Miranda, M., Kornacki, S., Wayne, M., Carr-Locke, D.L., and Theise, N.D. (2018). Structure and distribution of an unrecognized interstitium in human tissues. Sci. Rep. *8*, 4947.

Cano, E., Gebala, V., and Gerhardt, H. (2017). Pericytes or mesenchymal stem cells: is that the question? Cell Stem Cell *20*, 296–297.

(H–P) Flow-cytometry quantification of (H) blood and bone marrow or (I–P) lungs from tamoxifen-treated *N. brasiliensis*-infected mice at PI days 12–14 from the indicated strains (ASC-depleted and ASC-IL-33 Flox); ILC2s, eosinophils, Th2 cells, and Gata3^{hi} Treg cells were quantified.
Plots, images, or experiments in (A), (B), (D), (G), and (H) represent 2 or more mice. Data in (C) and (I)–(P) were pooled from greater than 3 experiments, and individual mice are shown. In (E) and (F), three individual mice were analyzed for each genotype. *$p < 0.05$; **$p < 0.01$; ns, not significant. Error bars represent means ± standard deviation. See also Figure S7.

Cayrol, C., and Girard, J.-P. (2018). Interleukin-33 (IL-33): A nuclear cytokine from the IL-1 family. Immunol. Rev. *281*, 154–168.

Chai, Q., Onder, L., Scandella, E., Gil-Cruz, C., Perez-Shibayama, C., Cupovic, J., Danuser, R., Sparwasser, T., Luther, S.A., Thiel, V., et al. (2013). Maturation of lymph node fibroblastic reticular cells from myofibroblastic precursors is critical for antiviral immunity. Immunity *38*, 1013–1024.

Chang, J.E., and Turley, S.J. (2015). Stromal infrastructure of the lymph node and coordination of immunity. Trends Immunol. *36*, 30–39.

Chen, W.-Y., Hong, J., Gannon, J., Kakkar, R., and Lee, R.T. (2015). Myocardial pressure overload induces systemic inflammation through endothelial cell IL-33. Proc. Natl. Acad. Sci. USA *112*, 7249–7254.

Corselli, M., Chen, C.-W., Sun, B., Yap, S., Rubin, J.P., and Péault, B. (2012). The tunica adventitia of human arteries and veins as a source of mesenchymal stem cells. Stem Cells Dev. *21*, 1299–1308.

Dalmas, E., Lehmann, F.M., Dror, E., Wueest, S., Thienel, C., Borsigova, M., Stawiski, M., Traunecker, E., Lucchini, F.C., Dapito, D.H., et al. (2017). Interleukin-33-activated islet-resident innate lymphoid cells promote insulin secretion through myeloid cell retinoic acid production. Immunity *47*, 928–942.e7.

de Kleer, I.M., Kool, M., de Bruijn, M.J.W., Willart, M., van Moorleghem, J., Schuijs, M.J., Plantinga, M., Beyaert, R., Hams, E., Fallon, P.G., et al. (2016). Perinatal activation of the interleukin-33 pathway promotes type 2 immunity in the developing lung. Immunity *45*, 1285–1298.

De Monte, L., Reni, M., Tassi, E., Clavenna, D., Papa, I., Recalde, H., Braga, M., Di Carlo, V., Doglioni, C., and Protti, M.P. (2011). Intratumor T helper type 2 cell infiltrate correlates with cancer-associated fibroblast thymic stromal lymphopoietin production and reduced survival in pancreatic cancer. J. Exp. Med. *208*, 469–478.

Durai, V., and Murphy, K.M. (2016). Functions of murine dendritic cells. Immunity *45*, 719–736.

Endo, Y., Hirahara, K., Iinuma, T., Shinoda, K., Tumes, D.J., Asou, H.K., Matsugae, N., Obata-Ninomiya, K., Yamamoto, H., Motohashi, S., et al. (2015). The interleukin-33-p38 kinase axis confers memory T helper 2 cell pathogenicity in the airway. Immunity *42*, 294–308.

Gerner, M.Y., Kastenmuller, W., Ifrim, I., Kabat, J., and Germain, R.N. (2012). Histo-cytometry: a method for highly multiplex quantitative tissue imaging analysis applied to dendritic cell subset microanatomy in lymph nodes. Immunity *37*, 364–376.

Gong, S., Zheng, C., Doughty, M.L., Losos, K., Didkovsky, N., Schambra, U.B., Nowak, N.J., Joyner, A., Leblanc, G., Hatten, M.E., and Heintz, N. (2003). A gene expression atlas of the central nervous system based on bacterial artificial chromosomes. Nature *425*, 917–925.

Guo, L., Huang, Y., Chen, X., Hu-Li, J., Urban, J.F., Jr., and Paul, W.E. (2015). Innate immunological function of TH2 cells in vivo. Nat. Immunol. *16*, 1051–1059.

Halim, T.Y.F., Hwang, Y.Y., Scanlon, S.T., Zaghouani, H., Garbi, N., Fallon, P.G., and McKenzie, A.N.J. (2016). Group 2 innate lymphoid cells license dendritic cells to potentiate memory TH2 cell responses. Nat. Immunol. *17*, 57–64.

Halim, T.Y.F., MacLaren, A., Romanish, M.T., Gold, M.J., McNagny, K.M., and Takei, F. (2012). Retinoic-acid-receptor-related orphan nuclear receptor alpha is required for natural helper cell development and allergic inflammation. Immunity *37*, 463–474.

Halim, T.Y.F., Rana, B.M.J., Walker, J.A., Kerscher, B., Knolle, M.D., Jolin, H.E., Serrao, E.M., Haim-Vilmovsky, L., Teichmann, S.A., Rodewald, H.-R., et al. (2018). Tissue-restricted adaptive type 2 immunity is orchestrated by expression of the costimulatory molecule OX40L on group 2 innate lymphoid cells. Immunity *48*, 1195–1207.e6.

Halim, T.Y.F., Steer, C.A., Mathä, L., Gold, M.J., Martinez-Gonzalez, I., McNagny, K.M., McKenzie, A.N.J., and Takei, F. (2014). Group 2 innate lymphoid cells are critical for the initiation of adaptive T helper 2 cell-mediated allergic lung inflammation. Immunity *40*, 425–435.

Han, X., Wang, R., Zhou, Y., Fei, L., Sun, H., Lai, S., Saadatpour, A., Zhou, Z., Chen, H., Ye, F., et al. (2018). Mapping the mouse cell atlas by Microwell-seq. Cell *172*, 1091–1107.e17.

Heredia, J.E., Mukundan, L., Chen, F.M., Mueller, A.A., Deo, R.C., Locksley, R.M., Rando, T.A., and Chawla, A. (2013). Type 2 innate signals stimulate fibro/adipogenic progenitors to facilitate muscle regeneration. Cell *153*, 376–388.

Kashiwagi, M., Hosoi, J., Lai, J.-F., Brissette, J., Ziegler, S.F., Morgan, B.A., and Georgopoulos, K. (2017). Direct control of regulatory T cells by keratinocytes. Nat. Immunol. *18*, 334–343.

Klose, C.S.N., and Artis, D. (2016). Innate lymphoid cells as regulators of immunity, inflammation and tissue homeostasis. Nat. Immunol. *17*, 765–774.

Koga, S., Hozumi, K., Hirano, K.-I., Yazawa, M., Terooatea, T., Minoda, A., Nagasawa, T., Koyasu, S., and Moro, K. (2018). Peripheral PDGFRα^{+}gp38^{+} mesenchymal cells support the differentiation of fetal liver-derived ILC2. J. Exp. Med. *215*, 1609–1626.

Kramann, R., Schneider, R.K., DiRocco, D.P., Machado, F., Fleig, S., Bondzie, P.A., Henderson, J.M., Ebert, B.L., and Humphreys, B.D. (2015). Perivascular Gli1+ progenitors are key contributors to injury-induced organ fibrosis. Cell Stem Cell *16*, 51–66.

Kumamoto, Y., Linehan, M., Weinstein, J.S., Laidlaw, B.J., Craft, J.E., and Iwasaki, A. (2013). CD301b^{+} dermal dendritic cells drive T helper 2 cell-mediated immunity. Immunity *39*, 733–743.

Lambrecht, B.N., and Hammad, H. (2017). The immunology of the allergy epidemic and the hygiene hypothesis. Nat. Immunol. *18*, 1076–1083.

McDavid, A., Finak, G., Chattopadyay, P.K., Dominguez, M., Lamoreaux, L., Ma, S.S., Roederer, M., and Gottardo, R. (2013). Data exploration, quality control and testing in single-cell qPCR-based gene expression experiments. Bioinformatics *29*, 461–467.

Miller, C.N., Hartigan-O'Connor, D.J., Lee, M.S., Laidlaw, G., Cornelissen, I.P., Matloubian, M., Coughlin, S.R., McDonald, D.M., and McCune, J.M. (2013). IL-7 production in murine lymphatic endothelial cells and induction in the setting of peripheral lymphopenia. Int. Immunol. *25*, 471–483.

Mohapatra, A., Van Dyken, S.J., Schneider, C., Nussbaum, J.C., Liang, H.-E., and Locksley, R.M. (2016). Group 2 innate lymphoid cells utilize the IRF4-IL-9 module to coordinate epithelial cell maintenance of lung homeostasis. Mucosal Immunol. *9*, 275–286.

Molofsky, A.B., Nussbaum, J.C., Liang, H.-E., Van Dyken, S.J., Cheng, L.E., Mohapatra, A., Chawla, A., and Locksley, R.M. (2013). Innate lymphoid type 2 cells sustain visceral adipose tissue eosinophils and alternatively activated macrophages. J. Exp. Med. *210*, 535–549.

Molofsky, A.B., Savage, A.K., and Locksley, R.M. (2015a). Interleukin-33 in tissue homeostasis, injury, and inflammation. Immunity *42*, 1005–1019.

Molofsky, A.B., Van Gool, F., Liang, H.-E., Van Dyken, S.J., Nussbaum, J.C., Lee, J., Bluestone, J.A., and Locksley, R.M. (2015b). Interleukin-33 and interferon-γ counter-regulate group 2 innate lymphoid cell activation during immune perturbation. Immunity *43*, 161–174.

Nussbaum, J.C., Van Dyken, S.J., von Moltke, J., Cheng, L.E., Mohapatra, A., Molofsky, A.B., Thornton, E.E., Krummel, M.F., Chawla, A., Liang, H.E., and Locksley, R.M. (2013). Type 2 innate lymphoid cells control eosinophil homeostasis. Nature *502*, 245–248.

Oboki, K., Ohno, T., Kajiwara, N., Arae, K., Morita, H., Ishii, A., Nambu, A., Abe, T., Kiyonari, H., Matsumoto, K., et al. (2010). IL-33 is a crucial amplifier of innate rather than acquired immunity. Proc. Natl. Acad. Sci. USA *107*, 18581–18586.

Oldham, M., Sakhalkar, H., Oliver, T., Allan Johnson, G., and Dewhirst, M. (2008). Optical clearing of unsectioned specimens for three-dimensional imaging via optical transmission and emission tomography. J. Biomed. Opt. *13*, 021113–021118.

Panduro, M., Benoist, C., and Mathis, D. (2016). Tissue Tregs. Annu. Rev. Immunol. *34*, 609–633.

Pichery, M., Mirey, E., Mercier, P., Lefrancais, E., Dujardin, A., Ortega, N., and Girard, J.-P. (2012). Endogenous IL-33 is highly expressed in mouse epithelial barrier tissues, lymphoid organs, brain, embryos, and inflamed tissues: in situ analysis using a novel Il-33-LacZ gene trap reporter strain. J. Immunol. *188*, 3488–3495.

Ricardo-Gonzalez, R.R., Van Dyken, S.J., Schneider, C., Lee, J., Nussbaum, J.C., Liang, H.-E., Vaka, D., Eckalbar, W.L., Molofsky, A.B., Erle, D.J., and Locksley, R.M. (2018). Tissue signals imprint ILC2 identity with anticipatory function. Nat. Immunol. *19*, 1093–1099.

Rodda, L.B., Lu, E., Bennett, M.L., Sokol, C.L., Wang, X., Luther, S.A., Barres, B.A., Luster, A.D., Ye, C.J., and Cyster, J.G. (2018). Single-cell RNA sequencing of lymph node stromal cells reveals niche-associated heterogeneity. Immunity *48*, 1014–1028.e6.

Saluzzo, S., Gorki, A.-D., Rana, B.M.J., Martins, R., Scanlon, S., Starkl, P., Lakovits, K., Hladik, A., Korosec, A., Sharif, O., et al. (2017). First-breath-induced type 2 pathways shape the lung immune environment. Cell Rep. *18*, 1893–1905.

Satija, R., Farrell, J.A., Gennert, D., Schier, A.F., and Regev, A. (2015). Spatial reconstruction of single-cell gene expression data. Nat. Biotechnol. *33*, 495–502.

Schraufnagel, D.E., Agaram, N.P., Faruqui, A., Jain, S., Jain, L., Ridge, K.M., and Sznajder, J.I. (2003). Pulmonary lymphatics and edema accumulation after brief lung injury. Am. J. Physiol. Lung Cell. Mol. Physiol. *284*, L891–L897.

Schuijs, M.J., and Halim, T.Y.F. (2018). Group 2 innate lymphocytes at the interface between innate and adaptive immunity. Ann. N Y Acad. Sci. *1417*, 87–103.

Shinoda, K., Hirahara, K., Iinuma, T., Ichikawa, T., Suzuki, A.S., Sugaya, K., Tumes, D.J., Yamamoto, H., Hara, T., Tani-Ichi, S., et al. (2016). Thy1+IL-7+ lymphatic endothelial cells in iBALT provide a survival niche for memory T-helper cells in allergic airway inflammation. Proc. Natl. Acad. Sci. USA *113*, E2842–E2851.

Sitnik, K.M., Wendland, K., Weishaupt, H., Uronen-Hansson, H., White, A.J., Anderson, G., Kotarsky, K., and Agace, W.W. (2016). Context-dependent development of lymphoid stroma from adult CD34(+) adventitial progenitors. Cell Rep. *14*, 2375–2388.

Stenmark, K.R., Yeager, M.E., El Kasmi, K.C., Nozik-Grayck, E., Gerasimovskaya, E.V., Li, M., Riddle, S.R., and Frid, M.G. (2013). The adventitia: essential regulator of vascular wall structure and function. Annu. Rev. Physiol. *75*, 23–47.

Vainchtein, I.D., Chin, G., Cho, F.S., Kelley, K.W., Miller, J.G., Chien, E.C., Liddelow, S.A., Nguyen, P.T., Nakao-Inoue, H., Dorman, L.C., et al. (2018). Astrocyte-derived interleukin-33 promotes microglial synapse engulfment and neural circuit development. Science *359*, 1269–1273.

Van Dyken, S.J., Mohapatra, A., Nussbaum, J.C., Molofsky, A.B., Thornton, E.E., Ziegler, S.F., McKenzie, A.N.J., Krummel, M.F., Liang, H.-E., and Locksley, R.M. (2014). Chitin activates parallel immune modules that direct distinct inflammatory responses via innate lymphoid type 2 and γδ T cells. Immunity *40*, 414–424.

Van Dyken, S.J., Nussbaum, J.C., Lee, J., Molofsky, A.B., Liang, H.-E., Pollack, J.L., Gate, R.E., Haliburton, G.E., Ye, C.J., Marson, A., et al. (2016). A tissue checkpoint regulates type 2 immunity. Nat. Immunol. *17*, 1381–1387.

Vivier, E., Artis, D., Colonna, M., Diefenbach, A., Di Santo, J.P., Eberl, G., Koyasu, S., Locksley, R.M., McKenzie, A.N.J., Mebius, R.E., et al. (2018). Innate lymphoid cells: 10 years on. Cell *174*, 1054–1066.

Yang, Y., Andersson, P., Hosaka, K., Zhang, Y., Cao, R., Iwamoto, H., Yang, X., Nakamura, M., Wang, J., Zhuang, R., et al. (2016). The PDGF-BB-SOX7 axis-modulated IL-33 in pericytes and stromal cells promotes metastasis through tumour-associated macrophages. Nat. Commun. *7*, 11385.

Ziegler, S.F. (2012). Thymic stromal lymphopoietin and allergic disease. J. Allergy Clin. Immunol. *130*, 845–852.

STAR★METHODS

KEY RESOURCES TABLE

REAGENT or RESOURCE	SOURCE	IDENTIFIER
Antibodies		
Anti-mouse CD45 BUV395 (clone 30-F11)	BD Biosciences	Cat#565967; RRID: AB_2739420
Anti-mouse CD45 PerCPCy5.5 (clone 30-F11)	Biolegend	Cat#103132; RRID: AB_893340
Anti-mouse CD45 BV421 (clone 30-F11)	Biolegend	Cat#103134; RRID: AB_2562559
Anti-mouse CD4 BV711 (clone RM4-5)	Biolegend	Cat#100557; RRID: AB_2562607
Anti-mouse CD8α BV786 (clone 53-6.7)	Biolegend	Cat#100750; RRID: AB_2562610
Anti-mouse CD8α Pacific Blue (clone 53-6.7)	Biolegend	Cat#100725; RRID: AB_493425
Anti-mouse CD3e Alexa700 (clone 17A2)	Biolegend	Cat#100216; RRID: AB_493697
Anti-mouse Siglec-F BV786 (clone E50-2440)	BD Biosciences	Cat#740956; RRID: AB_2740581
Anti-mouse CD11b BV605 (clone M1/70)	BD Biosciences	Cat#563015; RRID: AB_2737951
Anti-mouse CD11b Pacific Blue (clone M1/70)	Biolegend	Cat#101224; RRID: AB_755986
Anti-mouse F4/80 PE (clone BM8)	Biolegend	Cat#123110; RRID: AB_893486
Anti-mouse CD49b Pacific Blue (clone DX5)	eBioscience	Cat#108918; RRID: AB_2265144
Anti-mouse NK1.1 BV650 (clone PK136)	Biolegend	Cat#108736; RRID: AB_2563159
Anti-mouse NK1.1 Pacific Blue (clone PK136)	Biolegend	Cat#108722; RRID: AB_2132712
Anti-mouse CD19 PE/Dazzle594 (clone 6D5)	Biolegend	Cat#115554; RRID: AB_2564001
Anti-mouse CD19 Pacific Blue (clone 6D5)	Biolegend	Cat#115523; RRID: AB_439718
Anti-mouse CD25 PE (IL2Ra, clone PC61)	Biolegend	Cat#102008; RRID: AB_312857
Anti-mouse CD127 PECy7 (IL7Ra, clone A7R34)	Biolegend	Cat#135013; RRID: AB_1937266
Anti-mouse KLRG1 FITC (clone 2F1)	Biolegend	Cat#138410; RRID: AB_10643582
Anti-mouse CD90.2 BV421 (Thy1.2, clone 53-2.1)	Biolegend	Cat#140327; RRID: AB_2686992
Anti-mouse CD301b Alexa647 (clone URA-1)	Biolegend	Cat#146806; RRID: AB_2563388
Anti-mouse XCR1 Alexa647 (clone ZET)	Biolegend	Cat#148213; RRID: AB_2564368
Anti-mouse CD11c PECy7 (clone N418)	Biolegend	Cat#117318; RRID: AB_493568
Anti-mouse CD11c purified (clone N418)	Biolegend	Cat#117301; RRID: AB_313770
Anti-mouse MHCII (I-A/I-E, clone M5/114.15.2)	eBioscience	Cat#11-5321-85; RRID: AB_465233
Anti-mouse Gr-1 APCCy7 (clone RB5-8C5)	BD Biosciences	Cat#557661; RRID: AB_396775
Anti-mouse ST2 PE (clone DJ8)	MD Biosciences	Cat#101001PE
Anti-mouse Ly6C PerCPCy5.5 (clone HK1.4)	Biolegend	Cat#128011; RRID: AB_1659242
Anti-mouse TSLPR Fluorescein (polyclonal goat IgG)	R&D systems	Cat#FAB5461F; RRID: AB_2085207
Anti-mouse CD31 PE (clone 390)	Biolegend	Cat#102408; RRID: AB_312903
Anti-mouse CD31 biotin (clone 390)	Biolegend	Cat#102404; RRID: AB_312899
Anti-mouse CD31 purified (clone MEC13.3)	BD Biosciences	Cat#553370; RRID: AB_394816
Anti-mouse CD326 APCFire750 (EpCAM, clone G8.8)	Biolegend	Cat#118230; RRID: AB_2629758
Anti-mouse Ly6A/E BV711 (Sca-1, clone D7)	Biolegend	Cat#108131; RRID: AB_2562241
Anti-mouse Ly6A/E (Sca-1, clone D7) Alexa647	Life Technologies	Cat#MSCA21; RRID: AB_10375183
Anti-mouse Podoplanin (Gp38, clone 8.1.1)	Biolegend	Cat#127412; RRID: AB_10613648
Anti-mouse Lyve-1 eFluor660 (clone ALY7)	eBioscience	Cat#50-0443-82; RRID: AB_10597449
Anti-mouse PDGFR-α APC (CD140a, APA5)	Biolegend	Cat#135908; RRID: AB_2043970
Anti-mouse PDGFR-β APC (CD140b, APB5)	Biolegend	Cat#136007; RRID: AB_2043971
Anti-mouse CD124 PE (IL4Ra, clone REA235)	Miltenyi Biotec	Cat#130-102-710; RRID: AB_2654783
Anti-mouse FoxP3 PECy7 (clone FJK-16S)	eBioscience	Cat#25-5773-82; RRID: AB_891552
Anti-mouse Ki-67 FITC (clone 16A8)	Biolegend	Cat#652410; RRID: AB_2562141
Anti-mouse GATA3 eFluor660 (clone TWAJ)	eBioscience	Cat#50-9966-42; RRID: AB_10596663

(*Continued on next page*)

Continued

REAGENT or RESOURCE	SOURCE	IDENTIFIER
Anti-mouse IL-33 purified (polyclonal goat IgG)	R&D systems	Cat#AF3626; RRID: AB_884269
Anti-mouse TSLP purified (clone 152614)	R&D systems	Cat#MAB555-SP
Anti-mouse Aquaporin 5 (rabbit, polyclonal)	Abcam	Cat#ab78486; RRID: AB_1603410
Anti-mouse ColIV (rabbit, polyclonal)	Abcam	Cat#ab19808; RRID: AB_445160
Anti-mouse Alpha-smooth muscle actin Alexa488 (clone IA4)	eBioscience	Cat#53-9760-82; RRID: AB_2574461
Anti-mouse IL-4 purified (InVivoplus Mab, clone 11B11)	BioXcell	Cat#BP0045; RRID: AB_1107707
Anti-GFP (chicken, polyclonal)	Aves labs	Cat#GFP-1020; RRID: AB_10000240
Anti-DsRed (rabbit, polyclonal)	Clontech	Cat#632496; RRID: AB_10013483
Chemicals, Peptides, and Recombinant Proteins		
Draq7™	Biolegend	Cat#424001
Recombinant murine IL-1β	Biolegend	Cat#575102
Recombinant murine IL-4	Peprotech	Cat#214-14
Recombinant murine IL-7	R&D systems	Cat#407ML005
Recombinant murine IL-13	Peprotech	Cat#210-13
Recombinant murine IL-17A	Peprotech	Cat#210-17
Recombinant murine IL-33	Biolegend	Cat#580506
Recombinant murine TNFα	Peprotech	Cat#315-01A
Recombinant murine TSLP	R&D systems	Cat#555-TS-010
Recombinant murine PDGF-BB	Peprotech	Cat#315-18
Methyl Salicylate	Sigma	Cat#M6752
Tamoxifen	Sigma	Cat#T5648
Critical Commercial Assays		
LEGENDplex™ Mouse IL-5 Capture Bead	Biolegend	Cat#740056
LEGENDplex™ Mouse IL-13 Capture Bead	Biolegend	Cat#740060
LEGENDplex™ Mouse Th Cytokine Standard	Biolegend	Cat#740369
LEGENDplex™ Mouse TSLP Capture Bead	Biolegend	Cat#CMTSLPB4
LEGENDplex™ Mouse IL-33 Capture Bead	Biolegend	Cat#740144
LEGENDplex™ Mouse IL-7 Capture Bead	Biolegend	Cat#740141
LEGENDplex™ Mouse Custom Panel Standard Cocktail	Biolegend	custom
Dead Cell Apoptosis Kit with Annexin V Alexa Fluor™ 488 & Propidium Iodide (PI)	Invitrogen	Cat#V13241
CellTrace™ Violet Cell Proliferation Kit	Invitrogen	Cat#C34557
RNeasyPlus Micro kit	Qiagen	Cat#74034
SuperScript™ III First-Strand Synthesis System	Invitrogen	Cat#18080051
Power SYBR™ Green PCR Master Mix	Applied Biosystems	Cat#4367659
Zombie NIR™ Fixable Viability Kit	Biolegend	Cat#423105
DRAQ7	Biolegend	Cat#424001
CountBright™ Absolute Counting Beads	Invitrogen	Cat#C36950
Deposited Data		
Raw and analyzed data	This paper	GEO: GSE125492
Experimental Models: Organisms/Strains		
Mouse: B6(C)-*Il5*$^{tm1.1(icre)Lky}$/J (Red5)	Nussbaum et al., 2013	RRID: IMSR_JAX:030926
Mouse: B6.Cg-*Gt(ROSA)26Sor*$^{tm14(CAG-tdTomato)Hze}$/J (Ai14; R26-CAG-RFP)		RRID: IMSR_JAX:007914
Mouse: B6.*Il33*$^{mCherry/mCherry}$(IL-33mcherry)	Vainchtein et al., 2018	N/A
Mouse: B6.129S4-*Pdgfra*$^{tm11(EGFP)Sor}$/J (PDGFRαGFP)		RRID: IMSR_JAX:007669
Mouse: B6.Cg-*Foxp3*^{tm2Tch}/J (FoxP3GFP)		RRID: IMSR_JAX:006772
Mouse: *Il7*$^{eGFP/\ eGFP}$ (IL-7GFP)	Miller et al., 2013	N/A
Mouse: *Il33*$^{Gt/Gt}$ (*IL-33*$^{-/-}$)	Pichery et al., 2012	N/A

(*Continued on next page*)

Continued

REAGENT or RESOURCE	SOURCE	IDENTIFIER
Mouse: *Gli1*^{eGFP} (*Gli1*-GFP)	Gong et al., 2003	MGI:3843287
Mouse: *Ccl19*^{cre}(CCL19-cre)	Chai et al., 2013	MGI:5526991
Mouse: *Gli1*$^{tm3(cre/ERT2)Alj}$/J (*Gli1-cre*ERT2)		RRID: IMSR_JAX:007913
Mouse: B6.129P2-*Gt(ROSA)26Sor*$^{tm1(DTA)Lky}$/J (R26-DTA)		RRID: IMSR_JAX:009669
Mouse: B6.129X1-*Gt(ROSA)26Sor*$^{tm1(EYFP)Cos}$/J (R-YFP)		RRID: IMSR_JAX:006148
Mouse: *Il33*$^{Flox/Flox}$ (*Il33*$^{F/F}$)	Chen et al., 2015	N/A
Oligonucleotides		
Rps17(fwd) 5'-ATTGAGGTGGATCCCGACAC-3'	Elim biopharmaceuticals	N/A
Rps17(rev) 5'-TGCCAACTGTAGGCTGAGTG-3'	Elim biopharmaceuticals	N/A
Il33(fwd) 5'-AAGACCAGGTGCTACTACGC-3'	Elim biopharmaceuticals	N/A
Il33(rev) 5'-CTTCTTCCCATCCACACCGT-3'	Elim biopharmaceuticals	N/A
Col1a1(fw) 5'- TGACTGGAAGAGCGGAGAGT-3'	Elim biopharmaceuticals	N/A
Col1a1(rev) 5'- GTTCGGGCTGATGTACCAGT-3'	Elim biopharmaceuticals	N/A
Ccl11(fw) 5'-ATGAAAGGAGATGTGGGATTATT-3'	Elim biopharmaceuticals	N/A
Ccl11(rev) 5'- TTATCCTCAGTTACTCCTAACTCG-3'	Elim biopharmaceuticals	N/A
Software and Algorithms		
GraphPad Prism 7	GraphPad Software	N/A
FlowJo 10	Tree Star	N/A
Imaris 8.1 (Matlab plugin Sortomato)	Bitplane	N/A
Cell Ranger	10x Genomics	Version 1.3.1
Seurat	Satija et al., 2015	Version 1.4
R	https://www.r-project.org/	Version 3.4.4
RStudio	https://www.rstudio.com/	Version 1.0.143
Other		
Liberase TM	Roche	Cat#5401127001
DNase I	Roche	Cat#10104159001
Dispase II	Gibco	Cat#1710504
Collagenase I	Gibco	Cat#17100017
BD Pharm Lyse	BD Biosciences	Cat#555899
DAPI Fluoromount-G	Southern Biotech	Cat#0100-20

CONTACT FOR REAGENT AND RESOURCE SHARING

Further information and requests for resources and reagents should be delivered to and will be fulfilled by the Lead Contact, Ari B. Molofsky (ari.molofsky@ucsf.edu).

EXPERIMENTAL MODEL AND SUBJECT DETAILS

Mice

Red5 (*Il5-tdtomato*-cre) cytokine reporter mice were used for tracking IL-5-producing cells (Jackson 030926) (Nussbaum et al., 2013). For imaging Red5 mice were crossed to R26-CAG-RFP mice (Ai14) containing a flox-stop-flox sequence upstream of an CAG-RFP-WPRE- cassette in the constitutively expressed ROSA26 (R26) locus (Jackson 007914)). This strain marks all cells that have ever produced *Il5-cre* with tdtomato expression, serving as an IL-5 lineage-reporter. Additional mice utilized include genetically targeted IL-33mcherry (Vainchtein et al., 2018), PDGFRα-H2B-eGFP nuclear-localized GFP (Jackson 007669), FoxP3eGFP (tm2Tch) bicistronic mice (Jackson 006772), IL-7eGFP mice (Miller et al., 2013), IL-33 LacZ mice (Pichery et al., 2012), *Gli1*-GFP (Gong et al., 2003), Ccl19-Cre (Chai et al., 2013); R26-YFP, and *Gli1-cre-ERT2* mice (Jackson 007913) crossed with either R26-DTA (Diptheria toxin A, tamoxifen inducible cell deletion, Jackson 009669), R26-YFP mice (tamoxifen inducible lineage tracking, Jackson 006148), or IL-33 flox mice (Chen et al., 2015). To delete ILC2s, Red5 (*Il5-tdtomato*-cre) mice were intercrossed with R26-DTA, an approach that specifically deletes ~80% of ILC2s, as described previously (Nussbaum et al., 2013). All genetically targeted reporter strains were used in heterozygous state. Mice were mixed gender animals backcrossed on C57BL/6 for at least 10 generations, or on a mixed genetic

background (IL-33 flox, *Gli1-creERT2*). Mice were maintained in the UCSF specific pathogen–free animal facility in accordance with guidelines established by the Institutional Animal Care and Use Committee and Laboratory Animal Resource Center.

METHOD DETAILS

Flow cytometry

Whole lung was prepared by harvesting lung lobes into 5 ml HBSS with 0.2 mg/ml Liberase TM and 25 μg/ml DNase I, followed by automated tissue dissociation (GentleMacs; Miltenyi Biotec) using the ''lung1'' program, followed by tissue digestion for 30 min at 37°C with gentle agitation. Samples were subsequently processed on the GentleMacs using the ''lung2'' program, passed through 70μm filters, washed, and subjected to red blood cell lysis (PharmLyse; BD Biosciences) before final suspension in FACS buffer (PBS, 3% FCS, 0.05% NaN3). ILC2s were identified as lineage negative (CD11b$^-$, CD3ε$^-$, CD4$^-$, CD8α$^-$, CD19$^-$, NK1.1$^-$), FSC^{low}, SSC^{low}, CD45$^+$, Thy1.2 (CD90.2)$^+$, and Gata3^{hi}, IL1RL1 (ST2)$^+$, CD25 (IL-2Rα)$^+$, or KLRG1$^+$. In some cases, *Il5-tdtomato-cre*; R26-CAG-RFP (Ai14) mice were used to identify ILC2 as Lineage-, CD90+ RFP+. CD4$^+$ T cells were identified as FSC^{low} SSC^{low}, CD45$^+$, CD3ε$^+$, CD4$^+$. CD8$^+$ T cells were identified as FSC^{low} SSC^{low}, CD45$^+$, CD3ε$^+$, CD8$^+$. Eosinophils were identified as CD45$^+$, side-scatter high, DAPI-lo, CD11c$^-$, CD11b$^+$, and Siglec F$^+$. Tregs were identified as CD45$^+$ CD3ε$^+$ CD4$^+$ FoxP3$^+$. In some cases, FoxP3eGFP mice were used to identify Treg cell as GFP$^+$ CD3ε$^+$ CD4$^+$ cells. DCs were identified as CD45$^+$, CD19$^-$, NK1.1$^-$,SiglecF$^-$, Ly6G$^-$, Ly6C$^-$,CD11c$^+$ and MHCII^{high}. Epithelial cells were identified as CD45-, EpCAM+, CD31-. Endothelial cells were identified as CD45$^-$, CD31$^+$, EpCAM$^-$. Lymphatic endothelial cells were identified as CD45$^-$, CD31$^+$, EpCAM$^-$, Gp38$^+$. Mesenchymal stromal cells were identified as CD45$^-$ CD31$^-$ EpCAM$^-$, PDGFRα$^+$. In some cases, PDGFRαGFP mice were used to identify mesenchymal cells as CD45$^-$ CD31$^-$ EpCAM$^-$ GFP$^+$. Putative mesothelial cells were identified as CD45$^-$ EpCAM$^-$ CD31$^-$ PDGFRα$^-$ Sca1$^-$ Gp38^{hi}. Populations were back-gated to verify purity and gating. Samples were analyzed on an LSR II or, for cell sorting, a FACSAria II (both BD Biosciences). Live lymphocytes were gated by DAPI (4′,6-diamidine-2′-phenylindole dihydrochloride; Roche), Draq7 (Biolegend) (extracellular) or Zombie NIR fixable (Biolegend) (intracellular) exclusion, size and granularity based on forward- and side-scatter. Data were analyzed using FlowJo software (TreeStar, USA) and compiled using Prism (Graphpad Software). Cell counts were performed using flow cytometry counting beads (CountBright Absolute; Life Technologies) per manufacturer's instructions.

Flow cytometry Antibodies

Monoclonal antibodies used for flow cytometry include anti-CD4 (RM4-5, eBioscience and Biolegend), anti-Siglec-F (E50-2440, BD Pharmingen), anti-CD11b (M1/70; Biolegend), anti-F4/80 (BM8; eBioscience), anti-pan-NK (CD49b)(DX5; eBioscience), anti-NK1.1 (PK136, Biolegend or eBioscience or BD Bioscience), anti-FcεR1α (MAR-1; eBioscience or Biolegend), anti-CD3ε (17A2, BioLegend or eBioscience), anti-CD8α (53-6.7, Biolegend), anti-CD19 (1D3; BD-Pharmingen or Biolegend), anti-CD25 (IL2Ra, PC61, Biolegend), anti-CD127 (IL7Rα)(A7R34, eBioscience), anti-T1/ST2 (DJ8, MD Biosciences), anti-CD45 (30-F11, Biolegend), anti-KLRG1 (MAFA, Biolegend and eBioscience), and anti-CD90.2 (thy1.2)(30-H12, Biolegend), anti-301b (URA-1, Biolegend), anti-XCR1 (ZET, Biolegend), anti-CD11c (N418, Biolegend), anti-I-A/I-E (MHCII)(M5/114.15.2, Biolegend), anti-Ly6G (1A8, Biolegend), anti-Ly6C (HK1.4, Biolegend), anti-TSLPR (polyclonal, R&D systems). For non-hematopoietic cells, antibodies used include anti-CD31 (390, Biolegend, eBioscience), anti-EpCAM (CD326, G8.8, Biolegend), anti-Ly6A/E (Sca1, D7, eBioscience), anti-Gp38 (podoplanin)(8.1.1, Biolegend) , anti-Lyve1 (ALY7, eBioscience), anti-PDGFRα (CD140a, APA5, Biolegend), anti-CD124 (IL4Rα)(REA235, Miltenyi Biotech). Anti-FoxP3 (FJK-16S, eBiosciences), anti-Ki-67 (eBioscience) and anti-Gata3 (TWAJ, eBiosciences) were utilized after first using a fixable live/dead stain (Invitrogen), then fixing and permeabilizing cells per manufacturer's instructions.

Thin-Section Immunofluorescence microscopy

Animals were anesthetized and injected via intra-cardiac injection with 4% paraformaldehyde (PFA). Tissues were harvested and fixed for 2-4 h in 2% PFA, washed overnight with PBS, cryoprotected with 30% sucrose for 12-36 h, and embedded in OCT (Sakura Finetek) prior to freezing in blocks. For whole-mounts, tissues were fixed as above and imaged after permeabilization with 0.4% triton X and DAPI nuclear counterstaining. Frozen sections were processed on a Leica CM 3050S cryomicrotome (45 μm in VAT, 8 μm all others), dried on slides for 30 min, and kept at -80° C until staining. Tissues were blocked with 5% goat or horse serum (or other serum of secondary antibody) and maintained in PBS + 5% serum + 0.4% triton X throughout antibody treatments. Primary and secondary antibodies were incubated for 1 h at room temperature. Primary antibodies used include goat-anti IL-33 (R&D Systems, 1:100), anti-CD4 (RM4-5, Biolegend, 1:100), chicken anti-GFP (Aves labs, 1:500), rabbit anti-dsRed (Clontech, 1:500), rabbit anti-SMA (Abcam, 1:200), anti-Aqp5 (GR3200850-1, 1:200; Abcam, pAb), anti-Lyve1 (ALY7, 1:500 eBioscience), anti-Ly6A/E (Sca-1, MSCA21, Life Technologies), anti-CD3e (17A2, Biolegend, 1:100), anti-ColIV (diluted 1:200; Abcam), anti-MHCII I-A/I-E (M5/114.15.2, 1:100 eBiosiences), anti-CD11c (N418, Biolegend, 1:100), anti-CD45 (30-F11, Biolegend, 1:100), anti-human/mouse PDGFRα (BD Biosciences, 1:100), anti-PDGFRβ (APB5, Biolegend, 1:100). As necessary secondary antibodies were used at 1:1000 dilution at RT for 1 hour, conjugated to A488, A555, and A647 (Life Technologies, Thermo-Fisher). Slides were mounted with Vectashield hardset mounting media. Whole-mount tissue or slides were examined with a Zeiss AxioVision M2 fluorescent microscope.

3D Tissue Preparation and Imaging

Animals were sacrificed by lethal dose injection of avertin followed by cutting of the femoral artery. The lungs were subsequently inflated with 4% paraformaldehyde (PFA) via the trachea followed by clamping the trachea for 5 min. The lungs were then removed and

further fixed in agitated PFA for 10 min. During lung fixation other organs were removed and fixed in 4% PFA overnight at 4°C. Fixed tissues were cut into slices of approximately 300um using an in house built vibratome (Compresstome). Tissue slices were blocked, and permeabilized with 0.05% triton X, 10% FBS, and 1% BSA for 1-12 hrs at 4°C. Tissue was stained in fresh 700μL of 0.05 triton X, +10% FBS, 5% rat serum for primary antibodies, or appropriate species serum for secondary antibodies supplemented with antibodies and agitated at 4° C for 24hrs. For localization of ILC2s to anatomical structures, lung tissues were stained with anti-Lyve1 (ALY7, 1:500 eBioscience) and anti-SMA (IA4 1:500; Invitrogen) and in some cases, anti-CD31 (MEC13.3, 1:100, Biolegend). For localization of ILC2 cells to cuff regions the same stain was used with anti-Aquaporin 5 (1:200; Abcam, pAb, GR3200850-1). For localization of ILC2 cells with DCs, tissue slices were stained with anti-MHCII I-A/I-E (M5/114.15.2, 1:400 eBiosiences), anti-CD45 (30-F11, Biolegend, 1:250), anti-CD11c (N418, Biolegend, 1:200). For localization of ILC2s with stromal cell types, anti-SMA, Lyve1, and anti-IL-33 were used as described above. As necessary, species specific secondary antibodies were used (1:1000, Life Technologies) as described above. After overnight staining lung tissue was washed in PBS for 2 hrs followed by clearing and mounting in refractive index matching solution (RIMS). For adipose tissue, pancreas, meninges, kidney, and liver sections; slices were dehydrated in an ascending ethanol series (20–100%, 10 min each) and then cleared by soaking in methyl salicylate. All preparations were scanned using a Nikon A1R laser scanning confocal including 405, 488, 561, and 650 laser lines for excitation and imaging with 16x/0.8 or 25x1.1, NA Plan Apo long working distance water immersion objectives. Z steps were acquired every 2.5μm with an average of 200μm from the center of each slice imaged. Large surveys were acquired in resonant mode with pixel sizes of 900nm per pixel. High-resolution images were acquired in galvo mode with pixel sizes of 300nm and 2x frame averaging.

Image Analysis

Imaris Bitplane 8.1 was used for all 3D image analysis with the Imaris Matlab plugin Sortomato. For localization of ILC2s to anatomical structures in the lung colocalization channels were generated to represent different structures; airways (SMA alone), lymphatics (Lyve1 alone), blood vessels (SMA + Lyve1^{dim}). Each new channel was then surfaced and arteries and veins were further split based on anatomical location with arteries running parallel to the bronchioles and veins separated from bronchioles. ILC2s were then surfaced, and nearest neighbor analysis and distance analysis was conducted.

For ILC2 cuff localization in adults, SMA surfaces, Lyve1 surfaces (vessels) and Aquaporin 5 surfaces (parenchyma) were combined and pixels outside of the combined surfaces were masked to create a new channel representing the original empty spaces including, cuffs, lumens and alveolar spaces. Surfaces were analyzed on Sortomato, and non-cuff surfaces could be removed by a combination of volume, sphericity, surface area and distance to SMA.

For localizations of ILC2s with DCs, surfaces were generated on CD45 followed by analysis with Sortomato where DCs were selected as CD11c$^+$ and MHCII$^+$, AMs were selected as CD11c$^+$ and MHCII$^-$ with a sphericity greater than 0.8. ILC2s were identified by RFP expression. Localizations were measured using the surfaces interaction function of Sortomato with a 2X optical resolution cut off.

To localize ILC2s with different stromal cell types, colocalization channels were generated between DAPI$^+$ and green$^+$ pixels to represent PDGFRα$^+$ nuclei and DAPI- green+ for SMA. Surfaces could then be generated as described above. To parse PDGFRα subsets, a colocalization channel was made between PDGFRα and anti-IL-33. Surfaces were generated on PDGFRα$^+$ pixels. These surfaces were then sorted based on size and *median* colocalization of IL-33 and PDGFRα, which effectively excluded parenchymal stromal cells that appeared IL-33$^+$ due to a bright adjacent cell. This reveals the three PDGFRα$^+$ subsets of GFP-large IL-33$^-$, GFP-small IL-33$^-$, and GFP-small IL-33$^+$.

For developmental images, due to small numbers of ILC2s and compact airspaces, ILC2s were hand scored for localization within cuffs by examining their localization relative to the cuff surfaces in serial thin sections from confocal stacks. For distance quantitation for thin-cut sections, analysis was performed with a combination of ImageJ to define individual cells and python3 to measure the shortest distance between cells.

scRNAseq

Cells were purified from lung or adipose tissue and sorted for 1) all CD45$^-$ or 2) CD45$^-$ IL-33mcherry$^+$ cells and were run concurrently on the 10x Chromium (10x Genomics). The cells were partitioned into Gel Beads in Emulsion in the instrument, where cell lysis and barcoded reverse transcription of RNA occurred, followed by amplification, shearing and 5' adaptor and sample index attachment. Libraries were sequenced on an Illumina HiSeq 4000.

Data from 10x CellRanger were analyzed using R and the R package Seurat for single cell analysis (Satija et al., 2015). Cells were processed via the Seurat workflow to remove doublets and unwanted sources of variation by removing cells with more than 7000 genes per cell and regressing on number of UMIs. All genes expressed in fewer than three cells were filtered out, as were all cells that expressed fewer than 200 genes. The matrices of data were log normalized in a sparse data matrix and principal component analysis was performed to reduce dimensionality. The first 10 PCA components were used to cluster the cells by Louvain clustering implemented in Seurat while tSNE plots were independently generated to aid in 2D representation of multidimensional data independent of the clustering. This clustering method uses an optimization based on a KNN graph on Euclidean distance in the PCA space and processes the edge weights of pairs of cells based on their local neighbors. The 'bimod', likelihood-ratio test for single cell gene expression was used for differential gene analysis between the clusters to determine significant genes (McDavid et al., 2013). In cases where independent data sets were combined, we applied linear regression to the data sets to correct for batch effects prior

to running the pipeline described above. Log-normalized gene expression data was used for visualizations with violin plots (VlnPlot), tSNE plots (TSNEPlot), expression comparison plots (FeaturePlot), and generation of heatmaps (pheatmap (1.0.8)).

Induction of type 2 immune responses

For infections, 500 third-stage larvae of *N. brasiliensis* were injected subcutaneously as described (Molofsky et al., 2015b). Mice were killed at the indicated timepoints and tissues were harvested and analyzed. For cytokine injections, Interleukin-33 (R&D Systems) was given as 500 ng in 0.2 ml PBS i.p. every other day for three doses. Intranasal (i.n.) cytokine treatments was given for seven consecutive days, using 4μg of IL-13 and 2μg of IL-4 (both Peprotech). IL-4 was given in complex with anti-IL-4 mAb (BioXcell, clone 11B11, 10μg). For papain-induced type 2 immune responses, 10ug of papain was given i.n. in a total volume of 40μL for three consecutive days and lungs were analyzed four or eight days from the last treatment.

RNA preparation and qRT-PCR

Indicated populations were sorted into RLT Plus lysis buffer (Qiagen) and stored at -80°C, then processed using Allprep DNA/RNA micro kit (Qiagen) per manufacturer's protocol. For qPCR analyses, RNA was reverse transcribed using SuperScript III cDNA synthesis kit (ThermoFisher) and amplified using Power SYBR Green PCR master mix (ThermoFisher).

Mesenchymal – ILC2 co-cultures and cytokine analysis

Lungs from wild-type C57Bl/6 mice were harvested, manually dissociated with a razorblade, and subsequently digested with 7.5U/ml Dispase II, 114U/ml Collagenase I and 25μg/ml DNase I in PBS for 30 min at 37°C with gentle agitation. Samples were subsequently 1) washed with DMEM (supplemented with 10% FBS, 50U/mL penicillin and 50 μg /mL streptomycin) to obtain crude fibroblasts using a "walk-out" approach to culture adherent lung stromal cells or 2) passed through 70μm filters, washed, and subjected to red blood cell lysis (PharmLyse; BD Biosciences) before final suspension in FACS buffer (PBS, 3% FCS, 50U/mL penicillin and 50μg/mL streptomycin) to sort of PDGFRα$^+$ Sca1$^+$ and PDGFRα$^+$ Sca1$^-$ stroma (>98% purity). Stromal cells were seeded in flat-bottomed 96-well plates in 200μl DMEM (supplemented with 10% FBS, 50U/mL penicillin and 50 μg/mL streptomycin) at a density of 12,000 cells per well and allowed to form monolayers over 5-8 days. Lungs from IL-33-injected, *Il5-tdtomato-cre*; R26-CAG-RFP animals were pooled for ILC2 and T cell purification. Sorted ILC2s (lin$^-$, CD4$^-$, CD3$^-$, CD45$^+$ RFP$^+$), IL-5$^+$ Th2 cells (CD4$^+$, CD3$^+$, CD45$^+$ RFP$^+$), non-Th2 'antigen-experienced' CD4$^+$ T cells (CD4$^+$, CD3$^+$, CD44+, CD45$^+$ RFP$^-$) or non-Th2 'naive' CD4$^+$ T cells (lin$^-$, CD4$^+$, CD3$^+$, CD44$^-$, CD45$^+$ RFP$^-$, confirmed CD62L$^+$), were seeded onto the stromal monolayers or cultured with conditioned media from the stromal cell cultures in a total volume of 200μl, at a density of 3,000-10,000 ILC2s per well. In indicated experiments, ILC2s were labelled with 2.5uM CellTrace Violet (Invitrogen) to track proliferation. IL-2 (200U/mL), IL-7 (20ng/mL), IL-33 (10ng/mL) were added to culture media as a positive control and culture media only was used as negative control. After 3-8 days of culture, supernatants were collected, and cells were liberated, stained for CD45 and viability dye for dead cell exclusion, and analyzed and enumerated using CountBright Absolute counting beads (Life Technologies) by flow cytometry. In some experiments, wells were imaged by confocal microscopy or stained for AnnexinV to identify apoptotic cells. Indicated cytokines (TSLP (R&D Systems), IL-1β, IL-13, PDGF-BB, TNFα and IL-17A (Peprotech)) were added at a final concentration of 10ng/mL. TSLP and IL-33 were neutralized by addition of 1ug/mL anti-TSLP (R&Dsystems, clone 152614) or 1ug/mL anti-IL-33 (R&D systems, Polyclonal goat IgG), respectively. Amounts of IL-5, IL-7, IL-13, TSLP and IL-33 in cell culture supernatants were analyzed using LEGENDplex (BioLegend) according to the manufacturer's protocol.

QUANTIFICATION AND STATISTICAL ANALYSIS

All data were analyzed by comparison of means using unpaired two-tailed Student's t-tests using Prism, or for multiple comparisons ANOVA with Holm-Sidak post hoc test (GraphPad Software, La Jolla, CA), with *$p < 0.05$, **$p < 0.01$, ***$p < 0.001$. Figures display means ± standard deviation unless otherwise noted. When possible, results from independent experiments were pooled. All data points reflect individual biological replicates.

DATA AND SOFTWARE AVAILABILITY

The accession number for the scRNAseq data reported in this paper is GEO: GSE125492.